TIGHT BINDING MODELING OF TWO DIMENSIONAL AND QUASI-TWO DIMENSIONAL MATERIALS

A THESIS SUBMITTED TO
THE GRADUATE SCHOOL OF ENGINEERING AND SCIENCE
OF BILKENT UNIVERSITY
IN PARTIAL FULFILLMENT OF THE REQUIREMENTS FOR
THE DEGREE OF
MASTER OF SCIENCE
IN
PHYSICS

By
Deepak Kumar Singh
September 2017

Tight Binding Modeling of Two Dimensional and Quasi-Two Dimensional Materials
By Deepak Kumar Singh
September 2017

We certify that we have read this thesis and that in our opinion it is fully adequate, in scope and in quality, as a thesis for the degree of Master of Science.

Oğuz Gülseren(Advisor)

Mehmet Özgür Oktel

Süleyman Şinasi Ellialtoğlu

Approved for the Graduate School of Engineering and Science:

Ezhan Karaşan
Director of the Graduate School

ABSTRACT

TIGHT BINDING MODELING OF TWO DIMENSIONAL AND QUASI-TWO DIMENSIONAL MATERIALS

Deepak Kumar Singh
M.S. in Physics
Advisor: Oğuz Gülseren
September 2017

Since the advent of graphene, two-dimensional (2D) materials have consistently been studied owing to their exceptional electronic and optical properties. While graphene is completely two-dimensional in nature, its other analogues from the group IV A elements in the periodic table have been proven to have a low-buckled structure which adds up the exotic properties exhibited by them. The semiconductor industry is striving for such materials exhibiting exotic electronic, optical and mechanical properties.

In this thesis work we are primarily working towards a generalized tight-binding (TB) model for the 2D family of group IV A elements. Graphene has been studied extensively and we have successfully reproduced its energy band-structure accounting up to the third nearest neighbor contributions. The results have been checked extensively by performing simulations over a large set of available parameters and are found to be accurate. The other graphene analogues (viz; silicene, germanene and stanene) exhibiting a hexagonal 2D structure have been reported to have a buckling associated to them. We have analytically built up a TB model by considering the orbital projections along the bond length which accounts for the buckling in these 2D structures. Electronic band-structures have been reproduced and compared by taking into account the nearest neighbor and next-nearest neighbor contributions. Since these structures exhibit a Dirac like cone at the Dirac point and showing linear dispersion, study of electronic band-structures in detail becomes indispensable.

After the famous Kane and Mele paper on Quantum Spin Hall Effect in Graphene, condensed matter physicists have been looking for similar phenomena in other 2D materials. We have successfully included the spin-orbit coupling

(SOC) contribution to our unperturbed Hamiltonian and were able to produce splitting around the Dirac points. Since, Silicene and its other analogues exhibit same structure with different amount of buckling, we were able to track down the whole energy band-structure. Alongside this thesis also focuses on calculating optical properties of these materials.

In essence, this thesis work is an insight to the electronic and optical properties of the hexagonal 2D structures from the carbon family group. Derived structures from these 2D materials (viz; quantum dot, nano ribbon) could easily be studied utilizing the tight-binding formulation presented here. The proposed future work is the inclusion of nitrides and transition metal dichalcogenides (TMDCs) in the TB model.

Keywords: TB Model, Graphene, Spin-orbit coupling, Buckling, Electronic Band-Structure, Optical properties.

ÖZET

IKI BOYUTLU VE IKI BOYUTUMSU MALZEMELERIN SIKI BAĞ METODUYLA MODELLENMESI

Deepak Kumar Singh
Fizik Bölümü, Master
Tez Danışmanı: Oğuz Gülseren
Eylül 2017

Grafenin buluşundan itibaren, iki boyutlu (2B) malzemeler ilgina elektronik ve optik özellikleri dolayısıyla aktif bir araştırma alanı yaratmıştır. Grafen tamamen iki boyutlu bir malzemeyken, periyodik tablonun diğer IV-A grubu elementlerinin az-buruşuk yapıya sahip olduğu ve bu yapısal farklılığın elementlere bazı egzotik özellikler kazındırdıgı gösterilmıştır. Yarı iletken endüstrisinin yeni egzotik elektronik, optik ve mekanik özellikler sağlayacak yeni malzemeler bulma konusundaki çabaları bu araştırma alanının güncel ve önemli kılmaktadır.

Bu tez boyunca, genel sıkı bağlama metoduyla IV-A grubuna ait 2B malzemeler üzerinde çalışıldı. Geçmişte grafen hakkında yapılan kapsamlı çalışmalar örnek alınarak, grafenin üçüncü en yakın komşu katkıları da hesaba katılarak enerji bant yapısı başarıyla hesaplandı ve sonuçların doğruluğu birçok parametre göz önünde bulundurularak test edildi. Diğer iki boyutlu altıgen yapıya sahip grafen analoglarının (silicene, germanene, stanene gibi) buruşuk yapıya sahip oldukları literatürde bulunmaktadır. Biz, 2B malzemelerde buruşmaya sebep olan bağ uzunlukları boyunca bulunan orbital projeksiyonları da göz önünde bulundurarak sıkı bağlama modeli geliştirdik ve materyallerin elektronik bağ yapılarını bu analitik model ile tekrar oluşturarak sonuçları en yakın komşu ve bir sonraki en yakın komşu katkılarını da hesaba katarak karşılaştırdık. Bu tip yapılar Dirac noktasında Dirac benzeri koni şekli ve lineer dağılım gösterdiği için, elektronik bant yapısının detaylı olarak çalışılması çok önemlidir.

Kane ve Melenin Grafende kuvantum spin Hall etkisi hakkındaki meşhur makalelerinden sonra yoğun madde fizikçileri benzer olguyu diğer 2B malzemeler için de aramaya başlamıştır. Bu araştırmada biz, spin-orbit eşleşme katkısını bozulmamış Hamiltonian sistemimize başarıyla ekleyerek Dirac noktası

etrafındaki ayrılmayı gösterdik. Silisenin ve diğer analog malzemelerin farklı miktarlarda buruşma ve benzer yapısal özellikler göstermesi sebebiyle, bu araştırmada tüm enerji bant yapılarını detaylı olarak inceleyebilelik. Bunun yanı sıra, bu tez yukarıda bahsedilen malzemelerin optik özelliklerini hesaplamasının üzerinde de durmuştur.

Özet olarak, bu tez araştırması, karbon ailesi grubundaki altıgen 2B yapıların elektronik ve optik ozelliklerini detaylı olarak incelenmesı üzerinedır. Bu 2B malzemelerden türetilmiş yapılar (kuvantum noktası, nano şerit gibi) üzerine bu tezde sunulan sıkı bağlama metodundan faydalanarak kolayca çalışılabilir. Gelecek için önerilen çalışma konusu ise sunulan sıkı bağlama modeline nitritlerin ve geçiş metalleri dikalgocenitlerinin (TMDC) eklenmesi olabilir.

Anahtar sözcükler: Sıkı Bağlama Modeli, Grafen, Buruşma, Elektronik bant yapısı, optik özellikler.

Acknowledgement

I would like to express my sincere appreciation to my supervisor Prof. Oğuz Gülseren for his constant guidance and encouragement throughout the duration of this thesis work, without which the present form of thesis would not have been possible. It has been a great pleasure working under his supervision and I am truly grateful for his unwavering support.

I would also want to sincerely thanks Prof. Ceyhun Bulutay, who offered the course in atomic, molecular and optical physics. The lectures and discussions were very helpful in performing a significant part of calculations in this thesis, especially for the spin-orbit coupling part. I would like to extend my sincere gratitude to Assi. Prof. Seymur Cahangirov, fruitful discussions with him were very helpful in drafting this thesis.

A ton of thanks to my colleague and research group member Arash Mobaraki, who has always been there with a solution to my problem. Discussions with him have been eye-opening and his suggestions were of great help in carrying out computational part of this thesis. My sincere thanks to friends and colleagues, who made my stay at Bilkent University pleasant and memorable.

At last, it's my family members who have always been supporting and encouraging for all sort of endeavors and challenges I am facing or about to encounter. I owe you a great deal of thanks. A piece of thanks to my girlfriend Kavitha, who has always stood by my side in every situation for past many years.

Contents

List of Figures

List of Tables

Chapter 1

Introduction

Since the successful exfoliation of monolayer graphene sheet from graphite, courtesy to Novoselov and Geim for their stupendous discovery in the year 2004 [1], an extraordinary progress has been made in the past decade in the research of two-dimensional (2D) materials at the juncture of material science, chemistry and condensed matter physics. Exhibiting novel and extraordinary properties, these 2D materials have been investigated and explored in great detail for diverse potential applications. Given the unprecedented promises these 2D atomically thin sheets have on offer, the scientific community is probing deeper into the subject in order to understand and utilize their knowledge to the maximum possible extent.

Graphene is well known as a monolayer of carbon atoms, in which exists a 2D arrangement of these atoms to form a hexagonal lattice. It is considered as a building block for a variety of well known structures such as zero-dimensional (0D) fullerene, one-dimensional (1D) nanotubes and three-dimensional (3D) graphite (fig 1.1). Initial theoretical studies dates back to sixty years [2, 3, 4], where graphitic structures were investigated mostly for various aspects of its properties. For a very long time graphene was considered as a theoretical toy model and an academic material which could not exist in free state until an unexpected discovery of free standing graphene [1, 5] turned it into a reality. Experiments [1, 5] that followed this discovery confirmed the low energy charge carriers in graphene

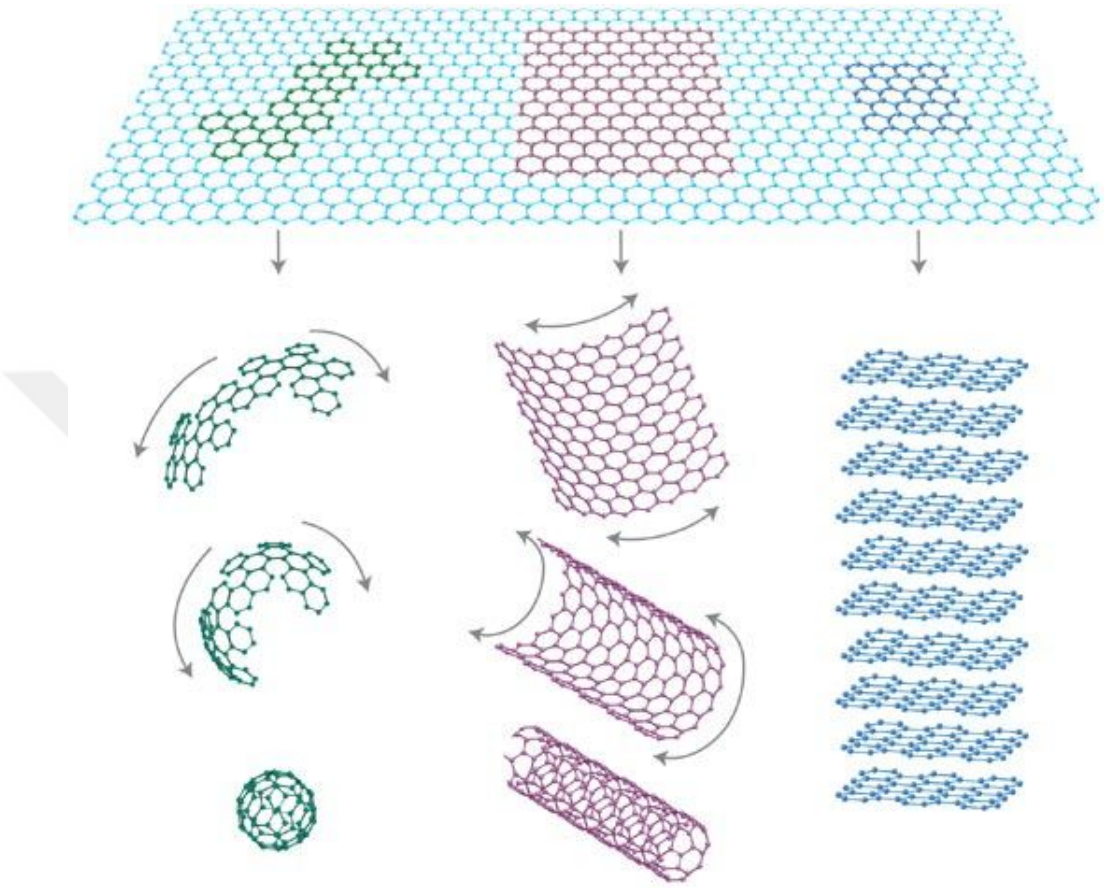

Figure 1.1: Graphene is a 2D building material for carbon materials of all other dimensions. It can be wrapped up into 0D buckyballs, rolled into 1D nanotubes or stacked into 3D graphite. [Adapted from Ref. [6]]

have a behavior of massless Dirac fermions.

The astonishing electronic, optical and mechanical properties of graphene has sparked a new virtue for exploring other similar 2D materials possessing similar structural features with multifaceted properties. Technological advancement in the fabrication methods for developing 2D ultrathin monolayers, of these methods a few are: mechanical cleavage [1, 5, 6, 8], chemical vapor deposition (CVD) [7], liquid exfoliation [9], anion exchange [14], microwave assisted oxidation [11, 12], hydrothermal self-assembly [13] and ion-intercalation [10] etc., have helped in realizing the conceived notion. At present, there exists a variety a these 2D

Parameters	C	Si	Ge	Sn
Lattice constant a ($\mathring{A}$)	2.46	3.86	4.06	4.67
Bond length ($\mathring{A}$)	1.42	2.23	2.34	2.69
Buckling ($\mathring{A}$)	0	0.45	0.69	0.85
Effective electronic mass m^* (m_0)	0	0.001	0.007	0.029
Energy gap (meV)	0.02	1.9	33	101

Table 1.1: Structural and electronic parameters for graphene, silicene, germanene and stanene. Adapted from Ref. [15]

structures such as transition metal dichalcogenides (TMDs), hexagonal boron nitrides (h-BN), phosphorene, analogues of graphene from group IV and MXenes. This thesis however has focused on tight-binding study of the electronic and optical properties of hexagonal honeycomb structures of carbon, silicon, germanium and tin.

1.1 Thesis Outline

Section 1 consists of introduction, where a brief history of graphene is discussed and a background is built for the framework of this thesis. In section 2, tight-binding model and its theory in which the secular equation has been presented. It is followed by a detailed explanation of vanishing and non-vanishing components of the Hamiltonian matrix. Spin-orbit coupling is introduced and the change it brings to the system under consideration is discussed next. Section 3 focuses on electronic properties of two-dimension materials from graphene upto stanene. Solution to the secular equation is found and band structures are plotted using available parameters. The next section investigates optical properties of these materials. Details for the calculation of optical absorption spectra along with gradient approximation method is presented. It is followed by the conclusion in

section 5, where future work is also discussed. Appendix A contains the dispersion function and direction cosines, needed for finding a solution to the secular equation. Appendix B presents the non-zero elements of perturbed Hamiltonian after considering spin-orbit interaction.

Chapter 2

Theory of the Tight-Binding Approximation

One of the most simplest method to calculate the band structure of a material is the Tight Binding Approximation (TBA), also sometimes called as Linear Combination of Atomic Orbitals (LCAO). TBA has long been available for electronic structure calculations since it was first proposed by Felix Bloch in 1928 [33]. Since it utilizes the symmetries and semi empirical formalism for parameters instead of explicit functions and exact forms, it often serves as an initial step in understanding the nature of electronic structure.

A key point in TBA is the concept of localized orbitals: The wavefunctions are understood in terms of a linear combination of highly localized atomic orbitals. This is followed by construction of Hamiltonian matrix, using a parameterised look-up table. While conceiving the Hamiltonian matrix elements, it is considered as an integral of three functions namely, one potential and two atomic orbitals centered at three sites. If all of these three functions are on the same site, it is regarded as one-center or on-site matrix element. In another possibility, if the orbitals are located on different sites and are neighbors to each other with potential on any of the two sites, gives us two-center matrix element or the on-site matrix element. Three center terms on different sites are neglected and it's the two-center approximation which forms a central thesis of the TBA. The parameterised two-center

form is implicit in the Slater-Koster table [34] and it allows TBA to express the dependence of hopping integrals upon distance analytically.

2.1 Tight-Binding Model

In a crystal, having lattice vectors defined as $\mathbf{a}_i$, translational symmetry along the directions of $\mathbf{a}_i$ makes the wavefunction to satisfy the Bloch's theorem, as

$$T\psi_k(r) = e^{i\mathbf{k}.\mathbf{a}_i}\psi_k(r) \tag{2.1}$$

where T is the translational operator in the direction of $\mathbf{a}_i$ and $\mathbf{k}$ is the Bloch wave vector [29]. Generally, in the tight binding model, single electron wave functions are expressed in terms of the atomic orbitals [30, 31]

$$\varphi_{nlm}(r,\theta,\Phi) = R_{nl}(r)\,Y_{lm}(\theta,\Phi) \tag{2.2}$$

where R_{nl} and Y_{lm} are radial and spherical harmonic functions in polar coordinates and n, l, m being the principal, angular momentum and magnetic quantum numbers respectively.
The wavefunction $\phi(k,r)$ on site j can be defined as a summation over the atomic wavefunctions $\phi(\mathbf{r}-\mathbf{R}_j)$

$$\phi_j(\mathbf{k},\mathbf{r}) = \frac{1}{\sqrt{N}}\sum_{\mathbf{R}_j}^{N} e^{i\mathbf{k}.\mathbf{R}_j}\varphi(\mathbf{r}-\mathbf{R}_j) \tag{2.3}$$

where $\mathbf{R}_j$ is the position of $j'th$ atom and N represents the number of atomic wavefunctions in the unit cell. The eigenfunctions in a crystal, can be defined as a linear combination of these Bloch functions as

$$\psi_j(\mathbf{k},\mathbf{r}) = \sum_{j'=1}^{n} C_{jj'}(\mathbf{k})\,\phi_j(\mathbf{k},\mathbf{r}) \tag{2.4}$$

where $C_{jj'}(\mathbf{k})$ are yet to be determined coefficients.
The eigenvalues of a physical system described by H is given as [32]

$$E_j(\mathbf{k}) = \frac{\langle\psi_j|H|\psi_j\rangle}{\langle\psi_j|\psi_j\rangle} = \frac{\int \psi_j^*(\mathbf{k},\mathbf{r})\,H\psi_j(\mathbf{k},\mathbf{r})\,dr}{\int \psi_j^*(\mathbf{k},\mathbf{r})\,\psi_j(\mathbf{k},\mathbf{r})\,dr} \tag{2.5}$$

Now, substituting $\phi_j(\mathbf{k},\mathbf{r})$ from equation (2.4) in the above equation

$$E_j\left(\mathbf{k}\right)=\frac{\sum_{j,j'=1}^{n}C_{ij}^{*}C_{ij'}\left\langle\phi_j|H|\phi_{j'}\right\rangle}{\sum_{j,j'=1}^{n}C_{ij}^{*}C_{ij'}\left\langle\phi_j|\phi_{j'}\right\rangle}=\frac{\sum_{j,j'=1}^{n}H_{jj'}\left(\mathbf{k}\right)C_{ij}^{*}C_{ij'}}{\sum_{j,j'=1}^{n}S_{jj'}\left(\mathbf{k}\right)C_{ij}^{*}C_{ij'}} \tag{2.6}$$

where $H_{jj'}\left(\mathbf{k}\right)$ and $S_{jj'}\left(\mathbf{k}\right)$ are known as the transfer and overlap matrices respectively and are defined as

$$\begin{aligned}H_{jj'}\left(\mathbf{k}\right)&=\left\langle\phi_j|H|\phi_{j'}\right\rangle\\S_{jj'}\left(\mathbf{k}\right)&=\left\langle\phi_j|\phi_{j'}\right\rangle\end{aligned} \tag{2.7}$$

The coefficient $C_{jj'}^{*}\left(\mathbf{k}\right)$ is optimized for a given $\mathbf{k}$ value in order to minimize $E_i\left(k\right)$ as follows

$$\begin{aligned}\frac{\partial E_i\left(\mathbf{k}\right)}{\partial C_{ij}^{*}\left(\mathbf{k}\right)}=&\frac{\sum_{j'=1}^{n}H_{jj'}\left(\mathbf{k}\right)C_{ij'}\left(\mathbf{k}\right)}{\sum_{j,j'=1}^{n}S_{jj'}\left(\mathbf{k}\right)C_{ij}^{*}(\mathbf{k})C_{ij'}\left(\mathbf{k}\right)}\\&-\frac{\sum_{j,j'=1}^{n}H_{jj'}\left(\mathbf{k}\right)C_{ij}^{*}\left(\mathbf{k}\right)C_{ij'}\left(\mathbf{k}\right)}{\left[\sum_{j,j'=1}^{n}S_{jj'}\left(\mathbf{k}\right)C_{ij}^{*}(\mathbf{k})C_{ij'}\left(\mathbf{k}\right)\right]^{2}}\sum_{j'=1}^{n}S_{jj'}\left(\mathbf{k}\right)C_{ij'}\left(\mathbf{k}\right)=0\end{aligned} \tag{2.8}$$

$$\begin{aligned}&\frac{\sum_{j'=1}^{n}H_{jj'}\left(\mathbf{k}\right)C_{ij'}\left(\mathbf{k}\right)}{\sum_{j,j'=1}^{n}S_{jj'}\left(\mathbf{k}\right)C_{ij}^{*}(\mathbf{k})C_{ij'}\left(\mathbf{k}\right)}\\&-\left[\frac{\sum_{j,j'=1}^{n}H_{jj'}\left(\mathbf{k}\right)C_{ij}^{*}\left(\mathbf{k}\right)C_{ij'}\left(\mathbf{k}\right)}{\sum_{j,j'=1}^{n}S_{jj'}\left(\mathbf{k}\right)C_{ij}^{*}(\mathbf{k})C_{ij'}\left(\mathbf{k}\right)}\right]\frac{\sum_{j'=1}^{n}S_{jj'}\left(\mathbf{k}\right)C_{ij'}\left(\mathbf{k}\right)}{\sum_{j,j'=1}^{n}S_{jj'}\left(\mathbf{k}\right)C_{ij}^{*}(\mathbf{k})C_{ij'}\left(\mathbf{k}\right)}=0\end{aligned} \tag{2.9}$$

Using equation (2.7) in the above

$$\sum_{j'=1}^{n}H_{jj'}\left(\mathbf{k}\right)C_{ij'}\left(\mathbf{k}\right)-E_i\left(\mathbf{k}\right)\sum_{j'=1}^{n}S_{jj'}\left(\mathbf{k}\right)C_{ij'}\left(\mathbf{k}\right)=0 \tag{2.10}$$

A matrix formulation of the equation can be given as

$$\left\{[H]-E_i\left(\mathbf{k}\right)[S]\right\}\left\{C_i\left(\mathbf{k}\right)\right\}=0 \tag{2.11}$$

A non-trivial solution of the above equation requires

$$\left|[H]-E_i\left(\mathbf{k}\right)[S]\right|=0 \tag{2.12}$$

Equation (2.12) is often known as the secular equation and it's eigenvalues $E_i(\mathbf{k})$ designates the electronic band structure of the system.

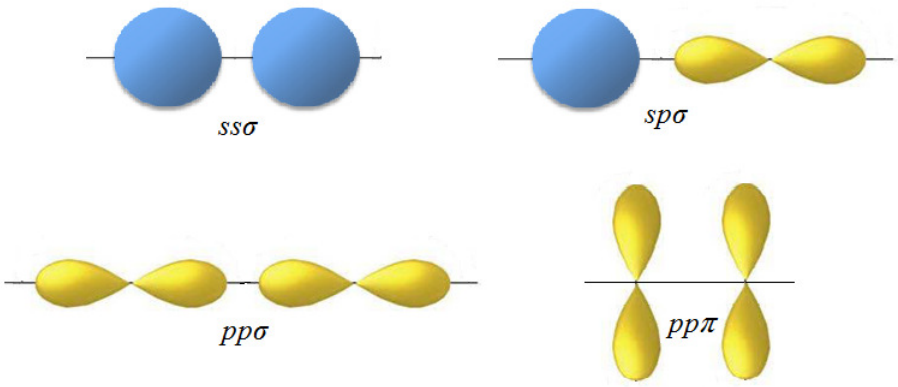

Figure 2.1: Non-vanishing matrix elements between s and p atomic orbitals in sp-bonding [Adapted from Ref. [35]]

2.2 Orbital Interaction in the Tight Binding Model

In the tight binding study of group IV elements in the periodic table, each element has four orbitals per atom in the outer shell, namely one s type and three p type (p_x, p_y, p_z) orbitals. In an orthogonal basis of atomic orbitals, for the purpose of solving the secular equation one needs to have a knowledge of Hamiltonian matrix elements formed due to orbital interactions at different interatomic sites. In the particular case where only s and p atomic orbitals are responsible for bonding, there exists only four non-zero overlap integrals as presented in figure 2.1. If the axis of the p orbital involved in sp-bonding is parallel (perpendicular) to the interatomic vector, it is called a σ (π) bond. Figure 2.2 represents the vanishing Hamiltonian matrix elements in the sp-bonding.

In general, the p orbitals are not just parallel or lie along the direction of atomic bonding as is depicted in figure (2.1) and (2.2). But, can also be oriented along different directions with respect to the bond length. In such cases, it becomes necessary to take projections of atomic orbitals in parallel and perpendicular direction to the bond length to account for the orbital interactions [36]. For example, while graphene is completely a two dimensional structure, its analogue

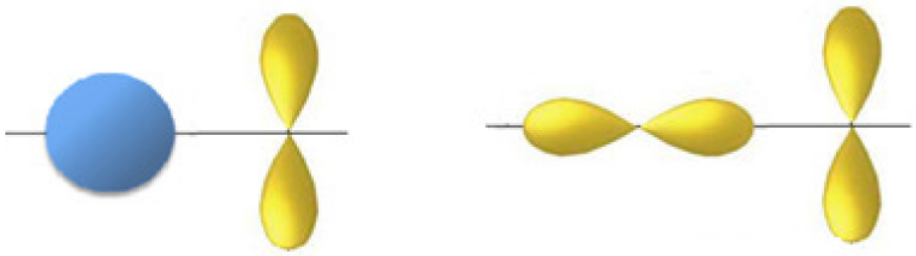

Figure 2.2: Vanishing matrix elements between s and p atomic orbitals corresponding to sp-bonding [Adapted from Ref. [35]]

from the same group have a buckled structure which in turn gives rise projections in all three direction. For this reason, a description of direction cosines becomes necessary and is presented here.

2.2.1 Projection corresponding to s and p atomic orbitals

A projection of p orbitals is required along the direction of bond length in order to achieve well defined orbital interactions. Each p orbital thus can be decomposed into two components: (1) parallel to the line joining the atomic orbitals and (2) perpendicular to the line joining the atomic orbitals. Figure (2.3) represents a randomly oriented p atomic orbital relative to the direction of bond length. If $\hat{\mathbf{d}}$ is the direction of bond length, $\hat{\mathbf{a}}$ is the unit vector along one of the Cartesian axes (x, y, z) and $\hat{\mathbf{n}}$ being the unit vector normal to the direction of $\hat{\mathbf{d}}$, each p orbital can then be decomposed into its parallel and normal components relative to $\hat{\mathbf{d}}$ as

$$\begin{aligned} |p_a\rangle &= \hat{\mathbf{a}}.\hat{\mathbf{d}}\,|p_d\rangle + \hat{\mathbf{a}}.\hat{\mathbf{n}}\,|p_n\rangle \\ &= cos\theta\,|p_d\rangle + sin\theta\,|p_n\rangle \end{aligned} \tag{2.13}$$

Thus, the Hamiltonian matrix element between an s orbital at one site and a p orbital on another atomic site would be presented as

$$\begin{aligned} \langle s|\mathbf{H}|p_a\rangle &= cos\theta\,\langle s|H|p_d\rangle + sin\theta\,\langle s|H|p_n\rangle \\ &= H_{sp\sigma}cos\theta \end{aligned} \tag{2.14}$$

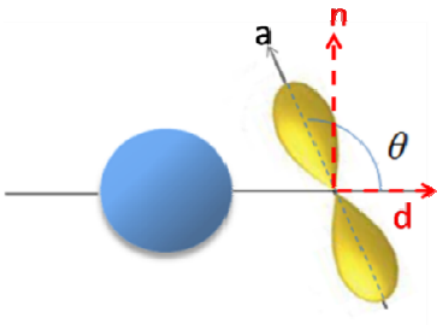

Figure 2.3: Orientation of p atomic orbital in random direction θ relative to the direction of bond length joining it to the s orbital [Adapted from Ref. [35]]

where the second term in above equation is a vanishing orbital interaction and is thus zero.

2.2.2 Projection corresponding to p and p atomic orbitals

For two p orbitals oriented along the directions of unit vectors $\hat{\mathbf{a}}_1$ and $\hat{\mathbf{a}}_2$ at angles θ_1 and θ_2 respectively, relative to the direction of line joining the two p orbitals represented by $\hat{\mathbf{d}}$ as depicted in figure (2.4), their decomposition in parallel and perpendicular directions could be given as

$$\begin{aligned} |p_a\rangle &= \hat{\mathbf{a}}_1.\hat{\mathbf{d}}\,|p_{d1}\rangle + \hat{\mathbf{a}}_1.\hat{\mathbf{n}}\,|p_{n1}\rangle \\ &= cos\theta_1\,|p_{d1}\rangle + sin\theta_1\,|p_{n1}\rangle \\ |p_b\rangle &= \hat{\mathbf{a}}_2.\hat{\mathbf{d}}\,|p_{d1}\rangle + \hat{\mathbf{a}}_2.\hat{\mathbf{n}}\,|p_{n1}\rangle \\ &= cos\theta_2\,|p_{d2}\rangle + sin\theta_2\,|p_{n2}\rangle \end{aligned} \tag{2.15}$$

Hamiltonian matrix element as a result of $p-p$ orbitals interactions from two different site can thus be presented as

$$\begin{aligned} \langle p_a|\mathbf{H}|p_b\rangle &= cos\theta_1 cos\theta_2\,\langle p_{d1}|\mathbf{H}|p_{d2}\rangle + sin\theta_1 sin\theta_2\,\langle p_{n1}|\mathbf{H}|p_{n2}\rangle \\ &= cos\theta_1 cos\theta_2 H_{pp\sigma} + sin\theta_1 sin\theta_2 H_{pp\pi} \end{aligned} \tag{2.16}$$

A general scheme for taking the projections can be defined in terms of direction

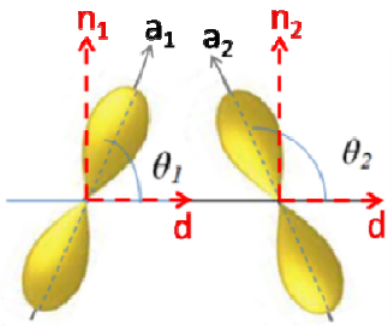

Figure 2.4: Orientation of two p atomic orbital in random direction θ relative to the direction of bond length joining them [Adapted from Ref. [35]]

cosines of p orbitals along the x, y and z axes as $\hat{\mathbf{d}} = (l_j, m_j, n_j)$.

$$\begin{aligned} l_j^{(n)} &= \frac{\widehat{i}.\delta_j^{(n)}}{|\delta_j^{(n)}|} \\ m_j^{(n)} &= \frac{\widehat{j}.\delta_j^{(n)}}{|\delta_j^{(n)}|} \\ n_j^{(n)} &= \frac{\widehat{k}.\delta_j^{(n)}}{|\delta_j^{(n)}|} \end{aligned} \tag{2.17}$$

where $\hat{i}, \hat{j}, \hat{k}$ are the unit vectors along the directions of x, y and z axes respectively and $\delta_j^{(n)}$ is coordinate of interacting orbital.

2.3 Spin-Orbit Interaction

Spin-orbit interaction is defined as an interaction which couples a particle's spin with its motion. Its a relativistic effect which breaks the degenerate energy states and causes fine structure of the atomic energy levels. A similar phenomena takes place in solid crystals leading to splitting of energy band structures.

2.3.1 L.S coupling

In the rest frame of nucleus, an electron does not experience any magnetic field acting on it. However, if the rest frame is reverted to electron, protons as charged particles creates an electric field around the atom, which in turn makes the electron experiencing a magnetic field

$$\mathbf{B} = -\frac{\mathbf{v} \times \mathbf{E}}{c^2} = \frac{\mathbf{v} \times \nabla V}{c^2} \tag{2.18}$$

where $\mathbf{v}$ is the velocity of electron with which it travels through the electric field $\mathbf{E}$, c is the speed of light and V is the potential. Since this electric field is spherically symmetric it depends on the distance r from the center of the nucleus as

$$\nabla V = \frac{\mathbf{r}}{r}\frac{dV}{dr} \tag{2.19}$$

The interaction due to the coupling of electron's spin and the magnetic field is given as [38]

$$U_{so} = \frac{e}{2m_e}\mathbf{S}.\mathbf{B} \tag{2.20}$$

where e is the electronic charge, m_e its mass and $\mathbf{S}$ is the spin operator. The factor 2 is due to the Thomas precession correction.

Equation (2.15) on substitution of equation (2.14) into equation (2.13) can be written as [37]

$$\begin{aligned} U_{so} &= \frac{e}{2m_e^2c^2}\mathbf{S}.\mathbf{v} \times \mathbf{r}\frac{1}{r}\frac{dV}{dr} \\ &= \frac{e}{2m_e^2c^2}\mathbf{S}.\mathbf{p} \times \mathbf{r}\frac{1}{r}\frac{dV}{dr} \\ &= -\frac{e}{2m_e^2c^2}\frac{1}{r}\frac{dV}{dr}\mathbf{L}.\mathbf{S} \\ &= \lambda\mathbf{L}.\mathbf{S} \end{aligned} \tag{2.21}$$

Here λ[1] represents all of the constants preceding $\mathbf{L}.\mathbf{S}$ and is a measure of the strength of the spin-orbit coupling. The value of λ can be estimated while treating it as a tight binding parameter.

The spin operator in the term $\mathbf{L}.\mathbf{S}$ can be expressed in terms of Pauli matrices as

$$\mathbf{L} = L_x\hat{i} + L_y\hat{j} + L_z\hat{k} \qquad\qquad \mathbf{S} = S_x\hat{i} + S_y\hat{j} + S_z\hat{k} \tag{2.22}$$

[1]Once we explicitly write the dot product $\mathbf{L}.\mathbf{S}$, λ eventually becomes $\lambda = -\frac{e\hbar}{2m_e^2c^2}\frac{1}{r}\frac{dV}{dr}$

$$S_x = \frac{\hbar}{2}\begin{bmatrix} 0 & 1 \\ 1 & 0 \end{bmatrix} \qquad S_y = \frac{\hbar}{2}\begin{bmatrix} 0 & -i \\ i & 0 \end{bmatrix} \qquad S_z = \frac{\hbar}{2}\begin{bmatrix} 1 & 0 \\ 0 & -1 \end{bmatrix} \tag{2.23}$$

The dot product **L**.**S** can then be expressed as

$$\begin{aligned} \mathbf{L}.\mathbf{S} &= L_x S_x + L_y S_y + L_z S_z \\ &= \frac{\hbar}{2}\begin{bmatrix} 0 & L_x \\ L_x & 0 \end{bmatrix} + \frac{\hbar}{2}\begin{bmatrix} 0 & -iL_y \\ iL_y & 0 \end{bmatrix} + \frac{\hbar}{2}\begin{bmatrix} L_z & 0 \\ 0 & -L_z \end{bmatrix} \\ &= \frac{\hbar}{2}\begin{bmatrix} L_z & L_x - iL_y \\ L_x + iL_y & -L_z \end{bmatrix} \\ &= \frac{\hbar}{2}\begin{bmatrix} L_z & L_- \\ L_+ & -L_z \end{bmatrix} \end{aligned} \tag{2.24}$$

where L_+ and L_- are known as the raising and lowering operators, respectively. For the magnetic quantum number m_l, the p orbitals can be decomposed in terms of $|m_l\rangle$ as

$$\begin{aligned} |p_x\rangle &= \frac{1}{\sqrt{2}}\left(|1\rangle + |-1\rangle\right) \\ |p_y\rangle &= \frac{1}{\sqrt{2}}\left(|1\rangle - |-1\rangle\right) \\ |p_z\rangle &= |0\rangle \end{aligned} \tag{2.25}$$

Action of operator L_z and ladder operators $L_\pm$ on state $|m_l\rangle$ gives

$$\begin{aligned} L_z\,|m_l\rangle &= l\,|m_l\rangle \\ L_\pm\,|m_l\rangle &= \hbar\sqrt{(l \mp m_l)\,(l \pm m_l + 1)}\,|m_l \pm 1\rangle \end{aligned} \tag{2.26}$$

In order to be able to find the matrix elements of the spin-orbit coupling, arbitrary eigenstates of the operator **L.S** can be given as

$$\begin{aligned}(\langle m_l,\uparrow| \quad \langle m_l,\downarrow|)\,\mathbf{L.S}\begin{pmatrix}|m_l^{'},\uparrow\rangle\\ |m_l^{'},\downarrow\rangle\end{pmatrix} =&\frac{\hbar}{2}\Big(\Big\langle m_l,\uparrow|L_z|m_l^{'},\uparrow\Big\rangle+\Big\langle m_l,\uparrow|L_-|m_l^{'},\downarrow\Big\rangle\\ &+\Big\langle m_l,\downarrow|L_+|m_l^{'},\uparrow\Big\rangle-\Big\langle m_l,\downarrow|L_z|m_l^{'},\downarrow\Big\rangle\Big)\end{aligned} \tag{2.27}$$

Since s and p orbitals are orthogonal to each other, every matrix element involving s orbital vanishes. One of the major changes brought in by the spin-orbit coupling is in the size of Hamiltonian matrix. The new basis for sp^3 hybridized structure becomes ($s_A^{\uparrow}$, $p_{xA}^{\uparrow}$, $p_{yA}^{\uparrow}$, $p_{zA}^{\uparrow}$, $s_B^{\uparrow}$, $p_{xB}^{\uparrow}$, $p_{yB}^{\uparrow}$, $p_{zB}^{\uparrow}$, $s_A^{\downarrow}$, $p_{xA}^{\downarrow}$, $p_{yA}^{\downarrow}$, $p_{zA}^{\downarrow}$, $s_B^{\downarrow}$, $p_{xB}^{\downarrow}$, $p_{yB}^{\downarrow}$, $p_{zB}^{\downarrow}$), which in turn gives rise to 16×16 Hamiltonian matrix. Non-zero elements of the spin-orbit interaction matrix elements need to be calculated between the p orbitals. Of the possible 36 terms, many are zero and a detailed calculation is presented in Appendix B. For our original Hamiltonian

$$H=\begin{bmatrix}H_{AA} & H_{AB}\\ H_{BA} & H_{BB}\end{bmatrix} \tag{2.28}$$

The resulting total Hamiltonian with spin-orbit interaction taken into consideration is

$$H=\begin{bmatrix}H_{AA}+SO_{\uparrow\uparrow} & H_{AB} & SO_{\uparrow\downarrow} & 0\\ H_{BA} & H_{AA}+SO_{\uparrow\uparrow} & 0 & SO_{\uparrow\downarrow}\\ SO_{\downarrow\uparrow} & 0 & H_{AA}+SO_{\downarrow\downarrow} & H_{AB}\\ 0 & SO_{\downarrow\uparrow} & H_{BA} & H_{AA}+SO_{\downarrow\downarrow}\end{bmatrix} \tag{2.29}$$

where

$$SO_{\uparrow\uparrow} = \lambda \begin{bmatrix} 0 & 0 & 0 & 0 \\ 0 & 0 & -i & 0 \\ 0 & i & 0 & 0 \\ 0 & 0 & 0 & 0 \end{bmatrix} \quad and \quad SO_{\uparrow\downarrow} = \lambda \begin{bmatrix} 0 & 0 & 0 & 0 \\ 0 & 0 & 0 & 1 \\ 0 & 0 & 0 & -i \\ 0 & -1 & i & 0 \end{bmatrix} \tag{2.30}$$

$SO_{\downarrow\uparrow} = SO'_{\uparrow\downarrow}$ and $SO_{\downarrow\downarrow} = SO'_{\uparrow\uparrow}$. Hopping elements in the total Hamiltonian H gives rise to block diagonal matrix while opposite spins couple to each other under influence of spin-orbit coupling. A noteworthy point here about the blocks due to hopping and onsite terms belonging to different spins is that they are identical. This causes the spin-up and spin-down bands to maintain their degeneracy. However, degeneracy is broken by $SO_{\uparrow\uparrow}$ and $SO_{\downarrow\downarrow}$ and bands are lifted.

Chapter 3

Properties of Two-Dimensional Materials

3.1 The Curious case of Graphene

Graphene is a one-atom-thick monolayer of sp^2 hybridized carbon atoms densely packed in a honeycomb crystal structure. It's hexagonal Bravais lattice consists of a two atom basis. Figure 3.1 illustrates the honeycomb structure of graphene lattice in real space. The unit cell consists of two carbon atoms at different sites. In this configuration, each carbon atom has three first nearest neighbours (1NN) from the other sublattice, six second nearest neighbours (2NN) or next-nearest neighbours from the same sublattice and three third-nearest neighbours (3NN) or next-to-next nearest neighbours from the other sublattice. The coordinates of 1NN carbon atoms are given as:

$$\delta_1^{(1)} = \left(\frac{a}{\sqrt{3}}, 0\right); \quad \delta_2^{(1)} = \left(-\frac{a}{2\sqrt{3}}, \frac{a}{2}\right); \quad \delta_3^{(1)} = \left(-\frac{a}{2\sqrt{3}}, -\frac{a}{2}\right) \tag{3.1}$$

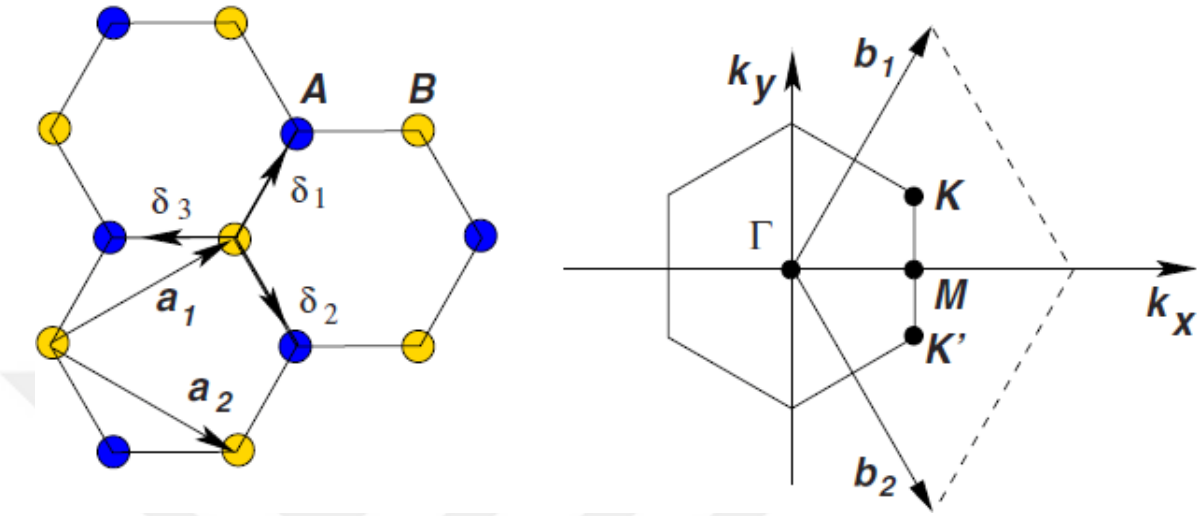

Figure 3.1: Hexagonal honeycomb lattice structure of graphene and its corresponding Brillouin zone. On left: three 1NN exists at site A (with their distances from the central atom denoted as δ_i) and six 2NN at site B. On right: Brillouin zone with symmetry points denoted as Γ, K and M. Formation of Dirac cones occur at K and $K^{'}$ points. Adapted from Ref. [23].

The coordinates of 2NN carbon atoms are:

$$\begin{aligned} \delta_1^{(2)} &= (0, a)\,; \quad \delta_2^{(2)} = (0, -a)\,; \\ \delta_3^{(2)} &= \left(\frac{\sqrt{3}a}{2}, -\frac{a}{2}\right); \quad \delta_4^{(2)} = \left(-\frac{\sqrt{3}a}{2}, \frac{a}{2}\right); \\ \delta_5^{(2)} &= \left(\frac{\sqrt{3}a}{2}, \frac{a}{2}\right); \quad \delta_6^{(2)} = \left(-\frac{\sqrt{3}a}{2}, -\frac{a}{2}\right) \end{aligned} \tag{3.2}$$

and the 3NN coordinates are given as:

$$\delta_1^{(3)} = \left(\frac{a}{\sqrt{3}}, a\right); \quad \delta_2^{(3)} = \left(\frac{a}{\sqrt{3}}, -a\right); \quad \delta_3^{(3)} = \left(-\frac{2a}{\sqrt{3}}, 0\right) \tag{3.3}$$

The bond length of a C-C bond or, in other words the nearest neighbour lattice distance in graphene is about $1.42\mathring{A}$ and the lattice constant has a value of $2.46\mathring{A}$. Each lattice in graphene has two sublattices namely A and B, and the unit vectors for these triangular sublattices are given as

$$\mathbf{a}_1 = \left(\frac{\sqrt{3}a}{2}, \frac{a}{2}\right), \quad \mathbf{a}_2 = \left(\frac{\sqrt{3}a}{2}, -\frac{a}{2}\right) \tag{3.4}$$

Electronic configuration of carbon atom is $1s^2 2s^2 2p^2$ and thus has four electrons in the outer shells. In graphene, the $2s$ and $2p$ levels of carbon atom mix up in a way

such that it gives rise to sp^2 hybridized structure. The $2s$ atomic orbital overlaps with the $2p_x$ and $2p_y$ atomic orbitals to produce three in-plane sp^2 hybridized orbitals with an occupancy of one electron in each three of them. The $2p_z$ atomic orbitals do not participate in this hybridization and remains singly occupied. The overlap of sp^2 hybridized orbitals is responsible for the formation of σ (σ^*) bonds, also known as bonding (anti-bonding) bonds. Being perpendicular to the plane, $2p_z$ atomic orbitals overlap sidewise and forms π (π^*) bonds, also known as bonding (anti-bonding) bonds.

The electronic band structure of graphene is dictated by σ and π bands which corresponds to σ and π bonds in the carbon atom respectively. Eight orbitals are at disposal to build the band structure inclusive of σ and π bands (σ^* and π^* bands) above the Fermi level (below the Fermi level). Considering the secular equation discussed in equation (2.12), the Hamiltonian matrix can be defined as in equation (3.5). The terms AA and AB depicts the integral between orbitals at the same site and different site respectively.

$$
\begin{aligned}
H &= \begin{bmatrix}
H_{11} & H_{12} & H_{13} & H_{14} & H_{15} & H_{16} & H_{17} & H_{18} \\
H_{21} & H_{22} & H_{23} & H_{24} & H_{25} & H_{26} & H_{27} & H_{28} \\
H_{31} & H_{32} & H_{33} & H_{34} & H_{35} & H_{36} & H_{37} & H_{38} \\
H_{41} & H_{42} & H_{43} & H_{44} & H_{45} & H_{46} & H_{47} & H_{48} \\
H_{51} & H_{52} & H_{53} & H_{54} & H_{55} & H_{56} & H_{57} & H_{58} \\
H_{61} & H_{62} & H_{63} & H_{64} & H_{65} & H_{66} & H_{67} & H_{68} \\
H_{71} & H_{72} & H_{73} & H_{74} & H_{75} & H_{76} & H_{77} & H_{78} \\
H_{81} & H_{82} & H_{83} & H_{84} & H_{85} & H_{86} & H_{87} & H_{88}
\end{bmatrix} \\
&= \begin{bmatrix}
H_{AA} & H_{AB} \\
H_{BA} & H_{BB}
\end{bmatrix}
\end{aligned}
\tag{3.5}
$$

$$
\begin{aligned}
H_{AA}(\mathbf{k}) &= \langle \phi_A | \mathbf{H} | \phi_A \rangle \\
&= \frac{1}{N} \sum_{\mathbf{R}_A}^{N} \sum_{\mathbf{R}'_A} e^{i\mathbf{k}.\left(\mathbf{R}_A - \mathbf{R}'_A\right)} \left\langle \varphi(\mathbf{r} - \mathbf{R}_A) | \mathbf{H} | \varphi\left(\mathbf{r} - \mathbf{R}'_A\right) \right\rangle \\
&= \frac{1}{N} \sum_{\mathbf{R}_A = \mathbf{R}'_A}^{N} \langle \varphi(\mathbf{r} - \mathbf{R}_A) | \mathbf{H} | \varphi(\mathbf{r} - \mathbf{R}_A) \rangle
\end{aligned}
\tag{3.6}
$$

In the sub-matrix H_{AA}, all non-diagonal terms are zero due to the spherical harmonics $Y_{lm}(\theta, \varphi)$ of p_x, p_y and p_z orbitals. The surviving diagonal terms are known as on-site matrix elements and are given as

$$
\begin{aligned}
H_{11}(k) &= \langle \phi_{2s} | \mathbf{H} | \phi_{2s} \rangle \\
&= \frac{1}{N} \sum_{\mathbf{R}_A = \mathbf{R}'_A}^{N} \langle \varphi_{2s}(\mathbf{r} - \mathbf{R}_A) | \mathbf{H} | \varphi_{2s}(\mathbf{r} - \mathbf{R}_A) \rangle = \varepsilon_{2s} \\
H_{22}(k) &= \langle \phi_{2p_x} | \mathbf{H} | \phi_{2p_x} \rangle \\
&= \frac{1}{N} \sum_{\mathbf{R}_A = \mathbf{R}'_A}^{N} \langle \varphi_{2p_x}(\mathbf{r} - \mathbf{R}_A) | \mathbf{H} | \varphi_{2p_x}(\mathbf{r} - \mathbf{R}_A) \rangle = \varepsilon_{2p} \\
H_{33}(k) &= \left\langle \phi_{2p_y} | \mathbf{H} | \phi_{2p_y} \right\rangle \\
&= \frac{1}{N} \sum_{\mathbf{R}_A = \mathbf{R}'_A}^{N} \left\langle \varphi_{2p_y}(\mathbf{r} - \mathbf{R}_A) | \mathbf{H} | \varphi_{2p_y}(\mathbf{r} - \mathbf{R}_A) \right\rangle = \varepsilon_{2p} \\
H_{44}(k) &= \langle \phi_{2p_z} | \mathbf{H} | \phi_{2p_z} \rangle \\
&= \frac{1}{N} \sum_{\mathbf{R}_A = \mathbf{R}'_A}^{N} \langle \varphi_{2p_z}(\mathbf{r} - \mathbf{R}_A) | \mathbf{H} | \varphi_{2p_z}(\mathbf{r} - \mathbf{R}_A) \rangle = \varepsilon_{2p}
\end{aligned}
\tag{3.7}
$$

Thus, the sub-matrix H_{AA} becomes

$$
H_{AA} = \begin{pmatrix}
\varepsilon_{2s} & 0 & 0 & 0 \\
0 & \varepsilon_{2p} & 0 & 0 \\
0 & 0 & \varepsilon_{2p} & 0 \\
0 & 0 & 0 & \varepsilon_{2p}
\end{pmatrix}
\tag{3.8}
$$

The sub-matrix H_{AB} is defined as

$$\begin{aligned} H_{AB}(\mathbf{k}) &= \langle \phi_A | \mathbf{H} | \phi_B \rangle \\ &= \frac{1}{N} \sum_{\mathbf{R}_A}^{N} \sum_{\mathbf{R}_B} e^{i\mathbf{k}.(\mathbf{R}_A - \mathbf{R}_B)} \langle \varphi(\mathbf{r} - \mathbf{R}_A) | \mathbf{H} | \varphi(\mathbf{r} - \mathbf{R}_B) \rangle \end{aligned} \tag{3.9}$$

The matrix elements in H_{AB} are due to the orbital interaction between different sites. Using coordinates of 1NN carbon atoms from equation (3.1), components of H_{AB} can be written as

$$\begin{aligned} H_{15}(\mathbf{k}) &= \langle \phi_{A2s} | \mathbf{H} | \phi_{B2s} \rangle \\ &= \frac{1}{N} \sum_{\mathbf{R}_A}^{N} \sum_{\mathbf{R}_B} e^{i\mathbf{k}.(\mathbf{R}_A - \mathbf{R}_B)} \langle \varphi_{A2s}(\mathbf{r} - \mathbf{R}_A) | \mathbf{H} | \varphi_{B2s}(\mathbf{r} - \mathbf{R}_B) \rangle \\ &= H_{ss\sigma} \sum_{i=1}^{3} e^{i\mathbf{k}.\mathbf{R}_{Ai}} \end{aligned} \tag{3.10}$$

where $\mathbf{R}_{Ai}$ is the vector joining atom A at one site to atoms B_i at other sites and the index i in $\mathbf{R}_{Ai}$ goes from 1 to 3 for 1NN.

Other matrix elements of H_{AB} are given as

$$\begin{aligned} H_{16}(\mathbf{k}) &= \langle \phi_{A2s} | \mathbf{H} | \phi_{B2p_x} \rangle \\ &= \frac{1}{N} \sum_{\mathbf{R}_A}^{N} \sum_{\mathbf{R}_B} e^{i\mathbf{k}.(\mathbf{R}_A - \mathbf{R}_B)} \langle \varphi_{A2s}(\mathbf{r} - \mathbf{R}_A) | \mathbf{H} | \varphi_{B2p_x}(\mathbf{r} - \mathbf{R}_B) \rangle \\ &= H_{sp\sigma} \sum_{i=1}^{3} e^{i\mathbf{k}.\mathbf{R}_{Ai}} cos\theta \end{aligned} \tag{3.11}$$

$$\begin{aligned} H_{17}(\mathbf{k}) &= \langle \phi_{A2s} | \mathbf{H} | \phi_{B2p_y} \rangle \\ &= \frac{1}{N} \sum_{\mathbf{R}_A}^{N} \sum_{\mathbf{R}_B} e^{i\mathbf{k}.(\mathbf{R}_A - \mathbf{R}_B)} \langle \varphi_{A2s}(\mathbf{r} - \mathbf{R}_A) | \mathbf{H} | \varphi_{B2p_y}(\mathbf{r} - \mathbf{R}_B) \rangle \\ &= H_{sp\sigma} \sum_{i=1}^{3} e^{i\mathbf{k}.\mathbf{R}_{Ai}} sin\theta \end{aligned} \tag{3.12}$$

$$
\begin{aligned}
H_{26}(\mathbf{k}) &= \langle \phi_{A2p_x} | \mathbf{H} | \phi_{B2p_x} \rangle \\
&= \frac{1}{N} \sum_{\mathbf{R}_A}^{N} \sum_{\mathbf{R}_B} e^{i\mathbf{k}.(\mathbf{R}_A - \mathbf{R}_B)} \langle \varphi_{A2p_x}(\mathbf{r} - \mathbf{R}_A) | \mathbf{H} | \varphi_{B2p_x}(\mathbf{r} - \mathbf{R}_B) \rangle \\
&= \sum_{i=1}^{3} \left[H_{pp\sigma} \cos^2\theta + H_{pp\pi} \left(1 - \cos^2\theta\right) \right] e^{i\mathbf{k}.\mathbf{R}_{Ai}}
\end{aligned} \tag{3.13}
$$

$$
\begin{aligned}
H_{27}(\mathbf{k}) &= \left\langle \phi_{A2p_x} | \mathbf{H} | \phi_{B2p_y} \right\rangle \\
&= \frac{1}{N} \sum_{\mathbf{R}_A}^{N} \sum_{\mathbf{R}_B} e^{i\mathbf{k}.(\mathbf{R}_A - \mathbf{R}_B)} \left\langle \varphi_{A2p_x}(\mathbf{r} - \mathbf{R}_A) | \mathbf{H} | \varphi_{B2p_y}(\mathbf{r} - \mathbf{R}_B) \right\rangle \\
&= \sum_{i=1}^{3} \left(H_{pp\sigma} - H_{pp\pi} \right) \cos\theta \sin\theta e^{i\mathbf{k}.\mathbf{R}_{Ai}}
\end{aligned} \tag{3.14}
$$

$$
\begin{aligned}
H_{37}(\mathbf{k}) &= \left\langle \phi_{A2p_y} | \mathbf{H} | \phi_{B2p_y} \right\rangle \\
&= \frac{1}{N} \sum_{\mathbf{R}_A}^{N} \sum_{\mathbf{R}_B} e^{i\mathbf{k}.(\mathbf{R}_A - \mathbf{R}_B)} \left\langle \varphi_{A2p_y}(\mathbf{r} - \mathbf{R}_A) | \mathbf{H} | \varphi_{B2p_y}(\mathbf{r} - \mathbf{R}_B) \right\rangle \\
&= \sum_{i=1}^{3} \left[H_{pp\sigma} \sin^2\theta + H_{pp\pi} \left(1 - \sin^2\theta\right) \right] e^{i\mathbf{k}.\mathbf{R}_{Ai}}
\end{aligned} \tag{3.15}
$$

$$
\begin{aligned}
H_{48}(\mathbf{k}) &= \langle \phi_{A2p_z} | \mathbf{H} | \phi_{B2p_z} \rangle \\
&= \frac{1}{N} \sum_{\mathbf{R}_A}^{N} \sum_{\mathbf{R}_B} e^{i\mathbf{k}.(\mathbf{R}_A - \mathbf{R}_B)} \langle \varphi_{A2p_z}(\mathbf{r} - \mathbf{R}_A) | \mathbf{H} | \varphi_{B2p_z}(\mathbf{r} - \mathbf{R}_B) \rangle \\
&= H_{pp\pi} \sum_{i=1}^{3} e^{i\mathbf{k}.\mathbf{R}_{Ai}}
\end{aligned} \tag{3.16}
$$

Other matrix elements of sub-matrix H_{AB} of the Hamiltonian matrix can be obtained utilizing the fact that: $\langle s|H|p\rangle = -\langle p|H|s\rangle$, $\langle p_A|H|p_B\rangle = \langle p_B|H|p_A\rangle$ and $\langle s_A|H|s_B\rangle = \langle s_B|H|s_A\rangle$. Sub-matrices H_{BA} and H_{BB} are given as

$$
H_{BA} = H_{AB}^{*} \quad and \quad H_{BB} = H_{AA} \tag{3.17}
$$

For the calculation of overlap integrals it is assumed that the atomic wavefunctions are normalized. The overlap matrix can be written in a similar way as that of the Hamiltonian matrix

$$
S = \begin{bmatrix} S_{AA} & S_{AB} \\ S_{BA} & S_{BB} \end{bmatrix}_{8\times 8} \tag{3.18}
$$

where each sub-matrix is a 4×4 matrix. Sub-matrix S_{AA} is a diagonal matrix with all diagonal elements equaling 1.

$$S_{AA} = \begin{pmatrix} 1 & 0 & 0 & 0 \\ 0 & 1 & 0 & 0 \\ 0 & 0 & 1 & 0 \\ 0 & 0 & 0 & 1 \end{pmatrix} \tag{3.19}$$

Matrix elements of S_{AB} are easy to find out, since matrix elements of H_{AB} are already known

$$\begin{aligned} S_{15} &= \langle \phi_{A2s} | \phi_{B2s} \rangle \\ &= S_{ss\sigma} \sum_{i=1}^{3} e^{i\mathbf{k}.\mathbf{R}_{Ai}} \end{aligned} \tag{3.20}$$

$$\begin{aligned} S_{16} &= \langle \phi_{A2s} | \phi_{B2p_x} \rangle \\ &= S_{sp\sigma} \sum_{i=1}^{3} e^{i\mathbf{k}.\mathbf{R}_{Ai}} \cos\theta \end{aligned} \tag{3.21}$$

$$\begin{aligned} S_{17} &= \left\langle \phi_{A2s} | \phi_{B2p_y} \right\rangle \\ &= S_{sp\sigma} \sum_{i=1}^{3} e^{i\mathbf{k}.\mathbf{R}_{Ai}} \sin\theta \end{aligned} \tag{3.22}$$

$$\begin{aligned} S_{26} &= \langle \phi_{A2p_x} | \phi_{B2p_x} \rangle \\ &= \sum_{i=1}^{3} \left[S_{pp\sigma} \cos^2\theta + S_{pp\pi} \left(1 - \cos^2\theta\right) \right] e^{i\mathbf{k}.\mathbf{R}_{Ai}} \end{aligned} \tag{3.23}$$

$$\begin{aligned} S_{27} &= \left\langle \phi_{A2p_x} | \phi_{B2p_y} \right\rangle \\ &= \sum_{i=1}^{3} \left(S_{sp\sigma} - S_{sp\pi} \right) \cos\theta \sin\theta e^{i\mathbf{k}.\mathbf{R}_{Ai}} \end{aligned} \tag{3.24}$$

$$\begin{aligned} S_{37} &= \left\langle \phi_{A2p_y} | \phi_{B2p_y} \right\rangle \\ &= \sum_{i=1}^{3} \left[S_{pp\sigma} \sin^2\theta + S_{pp\pi} \left(1 - \sin^2\theta\right) \right] e^{i\mathbf{k}.\mathbf{R}_{Ai}} \end{aligned} \tag{3.25}$$

Parameters	Value in eV
ϵ_{2s}	-8.70
ϵ_{2p}	0.00
$H_{ss\sigma}$	-6.70
$H_{sp\sigma}$	5.50
$H_{pp\sigma}$	5.10
$H_{pp\pi}$	-3.10
$S_{ss\sigma}$	0.20
$S_{sp\sigma}$	-0.10
$S_{pp\sigma}$	-0.15
$S_{pp\pi}$	0.12

Table 3.1: Tight binding parameters for graphene in the 1NN approximation obtained from Ref. [35]

$$\begin{aligned} S_{48} &= \langle \phi_{A2p_z} | \phi_{B2p_z} \rangle \\ &= S_{ss\pi} \sum_{i=1}^{3} e^{i\mathbf{k}.\mathbf{R}_{Ai}} \end{aligned} \tag{3.26}$$

Other matrix elements of sub-matrix S_{AB} of the overlap matrix can be obtained using the fact that: $\langle s|p\rangle = -\langle p|s\rangle$, $\langle p_A|p_B\rangle = \langle p_B|p_A\rangle$ and $\langle s_A|s_B\rangle = \langle s_B|s_A\rangle$. The tight-binding parameters are obtained by fitting the model to the electronic band structure obtained from experiments or *Ab-initio* calculations along the high symmetry points. Parameters used in this study are presented in the table (3.1) [35]. The electronic band structure of graphene, shown in figure (3.2), exhibits crossing of π bands at the K-point of the brillouin zone (BZ) at which point a linear dispersion is observed. In 3D visualization of the band structure, this linear band crossing occurs at K and K$'$ points of the first BZ. The high symmetry points along the $\Gamma - K - M - \Gamma$ direction defines the perimeter of a triangle inside the first BZ. Fermi level is defined at the zero of energy with bands above and below Fermi level representing anti-bonding and bonding bands respectively. The coordinates of high symmetry points are given as

$$\Gamma = (0,0)\,, \quad K = \frac{2\pi}{3a}\left(\sqrt{3}, 1\right), \quad M = \frac{2\pi}{3a}\left(\sqrt{3}, 0\right) \tag{3.27}$$

Neighboring site	ϵ_{2p}	$H^1_{pp\pi}$	$H^2_{pp\pi}$	$H^3_{pp\pi}$	$S^1_{pp\pi}$	$S^2_{pp\pi}$	$S^3_{pp\pi}$
1NN	0.00	-2.74			0.065		
2NN	-0.30	-2.77	-0.10		0.095	0.003	
3NN	-0.45	-2.78	-0.15	-0.095	0.117	0.004	0.002

Table 3.2: Tight binding parameters (all values in the table are in eV) for π-bands in graphene in the 1NN, 2NN and 3NN approximation obtained from Ref. [18].

The band structure of graphene at K-points closely resembles that of massless fermions in the Dirac spectrum [16, 17]. The reason behind considering the charge carriers in graphene to be imitating massless fermions relies on its crystal structure. Hopping between the two triangular sublattices results in forming two energy bands near the Fermi level and their intersection at the edges of BZ exhibits a conical behaviour. Unlike conventional semiconductors and metals, linear dispersion at Dirac points in graphene makes the quasiparticles behave differently.

Given the interesting feature of π-bands in graphene, a detailed explicit discussion of a reduced 2×2 Hamiltonian is presented here. For p_z orbitals interacting together, the effective Hamiltonian[1] is given as

$$H = \begin{bmatrix} H_{AA} & H_{AB} \\ H_{BA} & H_{BB} \end{bmatrix} \tag{3.28}$$

The solution of secular equation (2.12) with this Hamiltonian takes the following form

$$E_{\pm}(k) = \frac{\left[(2E_0 - E_1) \pm \sqrt{(E_1 - 2E_0)^2 - 4E_2E_3}\right]}{2E_3} \tag{3.29}$$

Where $E_0 = H_{AA}S_{AA,}$ $E_1 = H_{AB}S_{BA} + S_{AB}H_{BA}$, $E_2 = H_{AA}H_{BB} - H_{AB}H_{BA}$, and $E_3 = S_{AA}S_{BB} - S_{AB}S_{BA}$.

[1]The overlap matrix takes the similar form as the Hamiltonian matrix

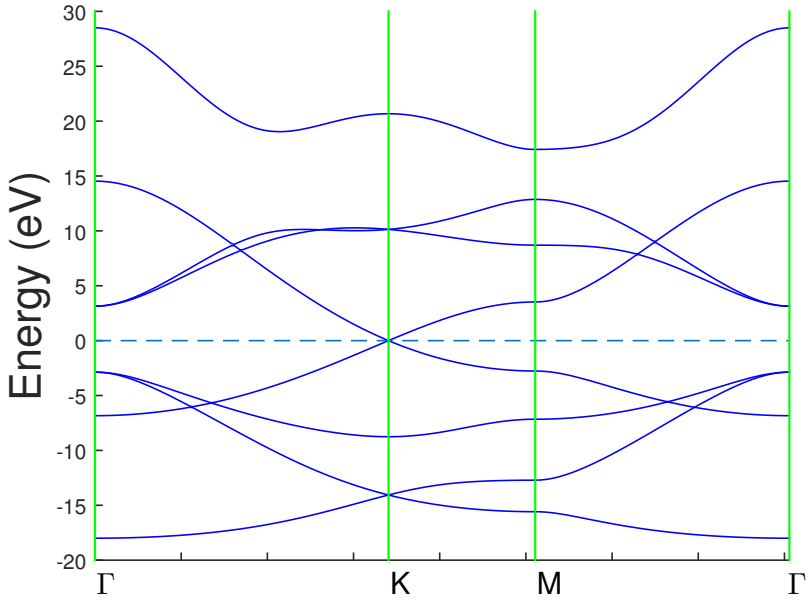

(a)

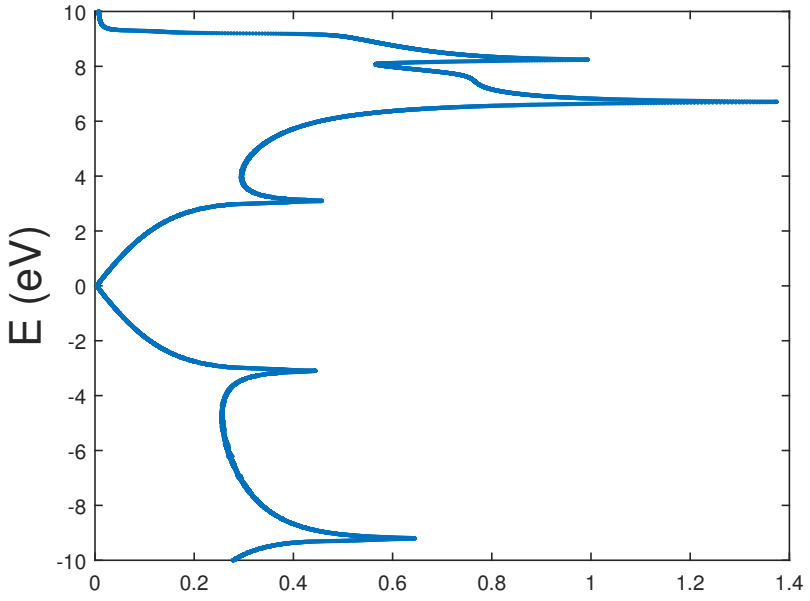

(b)

Figure 3.2: (a)Energy band structure of graphene drawn along the $\Gamma - K - M - \Gamma$ direction considering 1NN orbital interaction and (b) its corresponding DOS in the energy range $(-10eV \leq E \leq 10eV)$

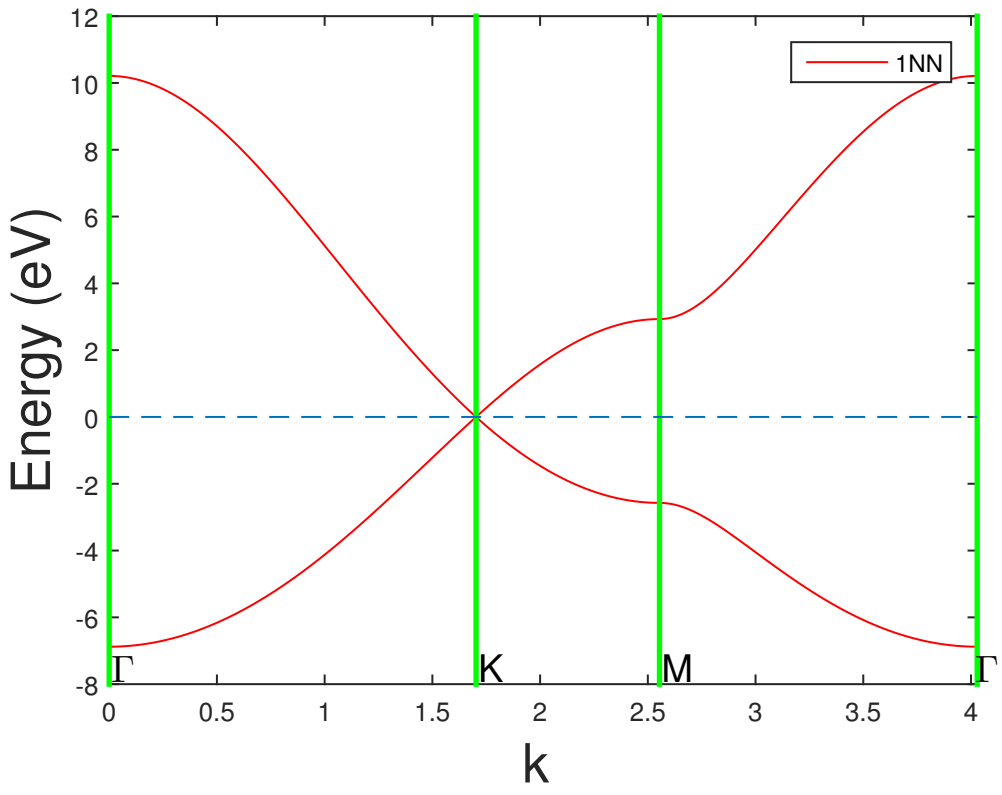

Figure 3.3: Electronic band structure of π bands in graphene from 1NN interaction

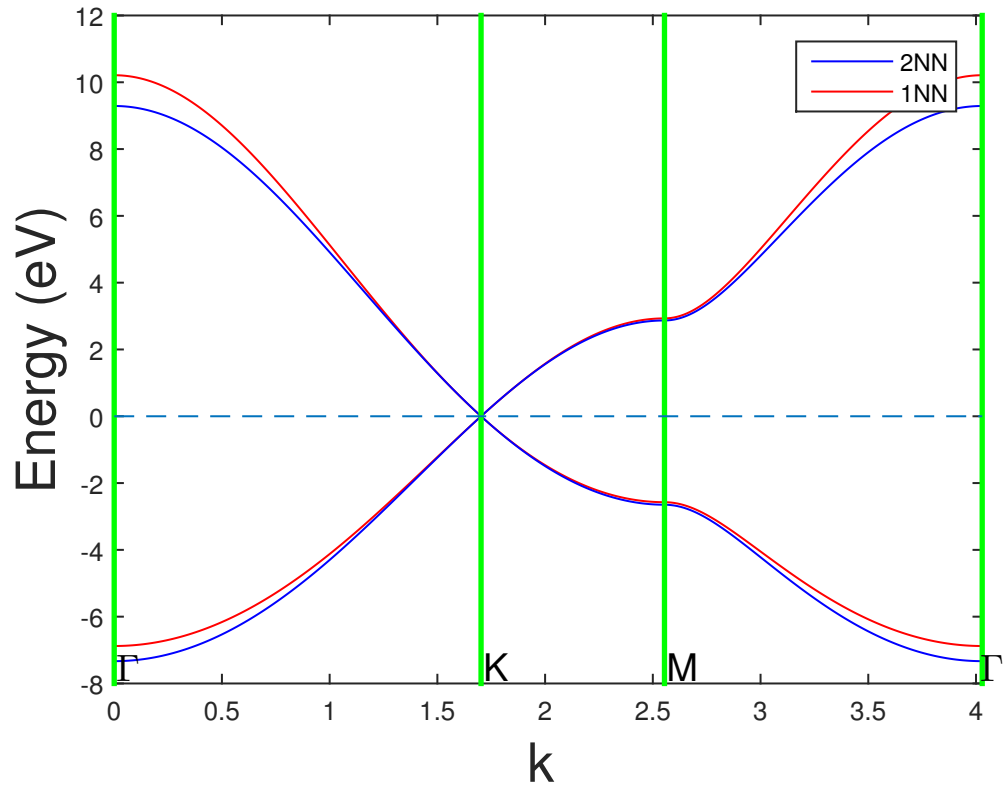

Figure 3.4: Electronic band structure of π bands in graphene from 1NN and 2NN interaction

In the 1NN approximation the eigen energies given in equation (3.29) takes the following form

$$E_{\pm}(\mathbf{k}) = \frac{\left[\left(\epsilon_{2p} - H^1_{pp\pi}S^1_{pp\pi}\right) \pm \left(H^1_{pp\pi} - S^1_{pp\pi}\epsilon_{2p}\right)\sqrt{g(\mathbf{k})}\right]}{1 - \left(S^1_{pp\pi}\right)^2 g(\mathbf{k})} \tag{3.30}$$

where $E_0 = \epsilon_{2p}$ and $g(\mathbf{k}) = 1 + 4\cos^2\left(\frac{k_y a}{2}\right) + 4\cos\left(\frac{\sqrt{3}k_x a}{2}\right)\cos\left(\frac{k_y a}{2}\right)$. In the 2NN approximation (only H_{AA} and S_{AA} matrix elements gets affected) the eigen energies given in equation (3.29) takes the following form

$$E_{\pm}(\mathbf{k}) = \frac{\left[\left(\epsilon_{2p} + H^2_{pp\pi}u(\mathbf{k}) \mp H^1_{pp\pi}g(\mathbf{k})\right)\right]}{1 + S^2_{pp\pi}u(\mathbf{k}) \mp S^1_{pp\pi}\sqrt{g(\mathbf{k})}} \tag{3.31}$$

where $u(\mathbf{k}) = 2\cos(k_y a) + 4\cos\left(\frac{\sqrt{3}k_x a}{2}\right)\cos\left(\frac{k_y a}{2}\right)$. Considering interaction upto 3NN (only H_{AB} and S_{AB} are the matrix elements that have changed) atomic sites

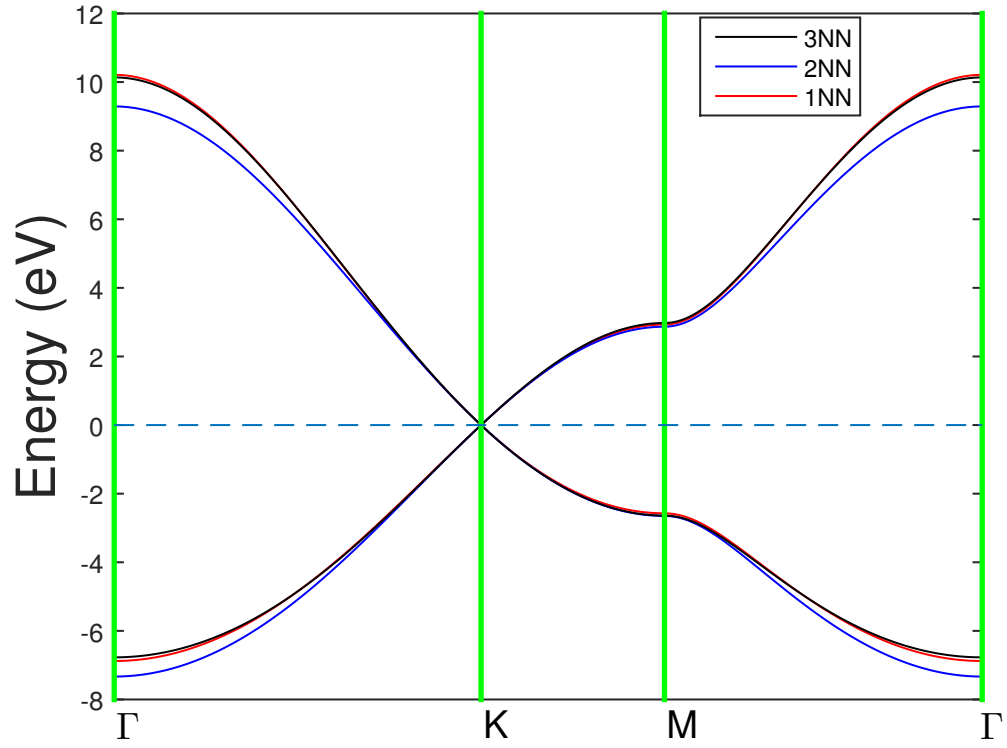

Figure 3.5: Electronic band structure of π bands in graphene for upto 3NN interaction

results in following values of E_1, E_2 and E_3 which produces eigen energies when substituted in equation (3.29)

$$\begin{aligned}
E_1 &= 2H^1_{pp\pi}S^1_{pp\pi}g\left(k\right) + \left(S^1_{pp\pi}H^3_{pp\pi}\right)t\left(k\right) + 2S^3_{pp\pi}H^3_{pp\pi}g\left(2k\right) \\
E_2 &= \left(\epsilon_{2p} + H^1_{pp\pi}u\left(k\right)\right)^2 - \left(\left(H^1_{pp\pi}\right)^2 g\left(k\right) + H^1_{pp\pi}H^3_{pp\pi}t\left(k\right) + \left(H^3_{pp\pi}\right)^2 f\left(k\right)\right) \\
E_2 &= \left(1 + S^2_{pp\pi}u\left(k\right)\right)^2 - \left(\left(S^1_{pp\pi}\right)^2 g\left(k\right) + S^1_{pp\pi}S^3_{pp\pi}t\left(k\right) + \left(S^3_{pp\pi}\right)^2 f\left(k\right)\right)
\end{aligned} \tag{3.32}$$

where $f\left(\mathbf{k}\right) = 1 + 4\cos^2\left(k_y a\right) + \cos\left(\sqrt{3}k_x a\right)\cos\left(k_y a\right)$ and $t\left(\mathbf{k}\right) = 2\cos\left(\sqrt{3}k_x a\right) + 4\cos\left(k_y a\right) + 4\cos\left(\frac{\sqrt{3}k_x a}{2}\right)\cos\left(\frac{k_y a}{2}\right) + 8\cos\left(\frac{\sqrt{3}k_x a}{2}\right)\cos\left(\frac{k_y a}{2}\right)\cos\left(k_y a\right)$.

3.2 Electronic Properties of Silicene

Moving down the group IV in periodic table along $C \rightarrow Si \rightarrow Ge \rightarrow Sn$, the atomic weight of these species increases drastically from $12 \rightarrow 119$. This in turn implies a stronger relativistic effect as the velocity of an electron in an atom is directly proportional to the atomic number. For similar systems having higher atomic numbers, as is discussed in the last section for graphene, the low energy physics could possibly be described by a Dirac type energy momentum relation.

Unlike carbon, the difference in energies of $3s$ and $3p$ atomic levels in silicon ($[Ne]3s^2 3p^2$) is nearly 5.66 eV (half of that for carbon), which opens up new horizons in π-bonding capabilities. As a result, Si thus utilizes all three p orbitals (namely p_x, p_y and p_z) resulting in a sp^3 hybridization. Given its proximity towards sp^3 hybridization, Si is more chemically reactive in comparison to C. One of the major differences between a planar sheet of C and Si lies in the fact that, due to its bigger atomic size silicene (monolayer sheet in which Si atoms are arranged in a periodic honeycomb lattice structure) becomes unstable in a planar structure. The competition between Si's affinity for sp^3 hybridization and graphene's affinity for sp^2 hybridization[2], results in a mixing of sp^2 and sp^3 hybridization schemes which incorporates as a non-zero buckling in silicene. Thus, the two neighboring atoms in silicene do not lie in the same plane, rather every alternate atom in silicene is buckled in the z-direction (if originally it was thought to lie in the xy-plane). Buckling in such distorted structures is defined as the distance between the two planes containing alternate atoms. Low ($0.44\mathring{A}$) and high ($2.15\mathring{A}$) buckled structures of silicene have been predicted [19, 20], where the low buckled structure is found to be more stable. However, in another piece of work [21] where a TB formulation is done assumes the stable buckling amounting to $0.78\mathring{A}$. In our analytical orthogonal TB formulation (overlap matrix turns into a identity matrix), we closely follow the approach of reference [21] in a sp^3

[2]The scheme of hybridization can be found out if the measures of bond angles are known and is given in terms of $\frac{1}{\cos\theta}$. For graphene, bond angle measures 120^o which returns a sp^2 hybridization scheme. In silicene, the measure of bond angle is 115.4^o, which falls between a sp^2 and sp^3 hybridisation.

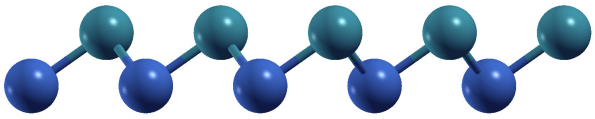

(a)

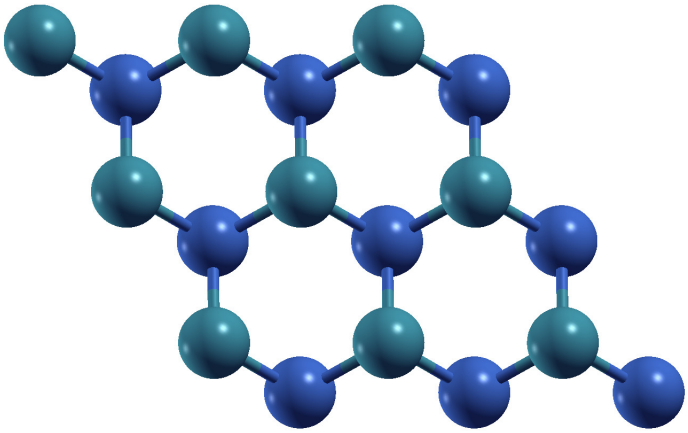

(b)

Figure 3.6: Figure (a) is arrangement of silicon-atoms in silicene seen from the top and figure (b) represents the real space lattice for silicene

hybridization[3] but occasionally retract from it wherever needed.

Coordinates of the 1NN atomic sites in silicene with a generalized buckling defined as Δ are

$$\delta_1^{(1)} = \left(\frac{a}{\sqrt{3}}, 0, \Delta\right); \quad \delta_2^{(1)} = \left(-\frac{a}{2\sqrt{3}}, \frac{a}{2}, \Delta\right); \quad \delta_3^{(1)} = \left(-\frac{a}{2\sqrt{3}}, -\frac{a}{2}, \Delta\right) \tag{3.33}$$

[3]Some authors have worked in a sp^3s^* hybridization scheme, where due to an additional s-orbital from the higher energy level the Hamiltonian matrix becomes a 10×10 matrix.

and for the 2NN atomic sites

$$\begin{aligned} \delta_1^{(2)} &= (0, a, 0)\,; & \delta_2^{(2)} &= (0, -a, 0)\,; \\ \delta_3^{(2)} &= \left(\frac{\sqrt{3}a}{2}, -\frac{a}{2}, 0\right); & \delta_4^{(2)} &= \left(-\frac{\sqrt{3}a}{2}, \frac{a}{2}, 0\right); \\ \delta_5^{(2)} &= \left(\frac{\sqrt{3}a}{2}, \frac{a}{2}, 0\right); & \delta_6^{(2)} &= \left(-\frac{\sqrt{3}a}{2}, -\frac{a}{2}, 0\right) \end{aligned} \tag{3.34}$$

In order to be able to get the energy dispersion relation for silicene, one must solve the secular equation as given by equation (2.12). Hamiltonian matrix here takes the same 8×8 form as presented in equation (3.5) but with different matrix elements which are produced in equation (3.35).

$$
\begin{aligned}
H_{11}(\mathbf{k}) &= \epsilon_{3s} + H^{AA}_{ss\sigma} g_{13}(\mathbf{k}) \\
H_{12}(\mathbf{k}) &= H^{AA}_{sp\sigma} g_{14}(\mathbf{k}) \\
H_{13}(\mathbf{k}) &= H^{AA}_{sp\sigma} g_{15}(\mathbf{k}) \\
H_{14}(\mathbf{k}) &= 0 \\
H_{15}(\mathbf{k}) &= H^{AB}_{ss\sigma} g_{0}(\mathbf{k}) \\
H_{16}(\mathbf{k}) &= H^{AB}_{sp\sigma} g_{1}(\mathbf{k}) \\
H_{17}(\mathbf{k}) &= H^{AB}_{sp\sigma} g_{2}(\mathbf{k}) \\
H_{18}(\mathbf{k}) &= H^{AB}_{sp\sigma} g_{8}(\mathbf{k}) \\
H_{22}(\mathbf{k}) &= \epsilon_{3p} + H^{AA}_{pp\sigma} g_{16}(\mathbf{k}) + H^{AA}_{pp\pi} g_{17}(\mathbf{k}) \\
H_{23}(\mathbf{k}) &= \left(H^{AA}_{pp\sigma} - H^{AA}_{pp\pi}\right) g_{18}(\mathbf{k}) \\
H_{24}(\mathbf{k}) &= 0 \\
H_{26}(\mathbf{k}) &= H^{AB}_{pp\sigma} g_{3}(\mathbf{k}) + H^{AB}_{pp\pi} g_{4}(\mathbf{k}) \\
H_{27}(\mathbf{k}) &= \left(H^{AB}_{pp\sigma} - H^{AB}_{pp\pi}\right) g_{5}(\mathbf{k}) \\
H_{28}(\mathbf{k}) &= \left(H^{AB}_{pp\sigma} - H^{AB}_{pp\pi}\right) g_{9}(\mathbf{k}) \\
H_{33}(\mathbf{k}) &= \epsilon_{3p} + H^{AA}_{pp\sigma} g_{19}(\mathbf{k}) + H^{AA}_{pp\pi} g_{20}(\mathbf{k}) \\
H_{34}(\mathbf{k}) &= 0 \\
H_{37}(\mathbf{k}) &= H^{AB}_{pp\sigma} g_{6}(\mathbf{k}) + H^{AB}_{pp\pi} g_{7}(\mathbf{k}) \\
H_{38}(\mathbf{k}) &= \left(H^{AB}_{pp\sigma} - H^{AB}_{pp\pi}\right) g_{10}(\mathbf{k}) \\
H_{44}(\mathbf{k}) &= \epsilon_{3p} + H^{AA}_{pp\pi} g_{25}(\mathbf{k}) \\
H_{48}(\mathbf{k}) &= H^{AB}_{pp\sigma} g_{11}(\mathbf{k}) + H^{AB}_{pp\pi} g_{12}(\mathbf{k})
\end{aligned}
\tag{3.35}
$$

where the values for dispersion functions $g_i(\mathbf{k})$ $(for \quad i = 1, 2, \ldots, 25)$ are produced in appendix A. Other matrix elements of Hamiltonian H can be found easily from the values of already found matrix elements utilizing the fact that: $\langle s|H|p\rangle = -\langle p|H|s\rangle$ and $\langle p_A|H|p_B\rangle = \langle p_B|H|p_A\rangle$. The low energy effective Hamiltonian including the π bands can be written as follows

$$
H(\mathbf{k}) = \begin{bmatrix} \epsilon_{3p} + H^{AA}_{pp\pi} g_{25}(\mathbf{k}) & H^{AB}_{pp\pi} g_{12}(\mathbf{k}) \\ H^{AB}_{pp\pi} g^{*}_{12}(\mathbf{k}) & \epsilon_{3p} + H^{AA}_{pp\pi} g_{25}(\mathbf{k}) \end{bmatrix}
\tag{3.36}
$$

Parameters	Value in eV
ϵ_{3s}	-4.0497
ϵ_{3p}	-1.0297
$\mathrm{H}_{ss\sigma}^{AB}$	-2.0662
$\mathrm{H}_{sp\sigma}^{AB}$	2.0850
$\mathrm{H}_{pp\sigma}^{AB}$	3.1837
$\mathrm{H}_{pp\pi}^{AB}$	-0.9488
$\mathrm{H}_{ss\sigma}^{AA}$	0.0000
$\mathrm{H}_{sp\sigma}^{AA}$	0.0000
$\mathrm{H}_{pp\sigma}^{AA}$	0.8900
$\mathrm{H}_{pp\pi}^{AA}$	-0.3612

Table 3.3: Tight binding parameters for silicene in the 2NN approximation obtained from Ref. [21, 22]

This Hamiltonian can be solved for the eigen-energies to obtain the following energy dispersion relation of *pi*-bands as

$$E_{\pm}\left(\mathbf{k}\right) = \epsilon_{3p} + H_{pp\pi}^{AA} g_{25}\left(\mathbf{k}\right) \pm H_{pp\pi}^{AB} \left|g_{12}\left(\mathbf{k}\right)\right| \tag{3.37}$$

Figure (3.7) presents 8-band band structure of silicene in two buckling configurations[4], namely $\Delta = 0.44\mathring{A}$ and $\Delta = 0.78\mathring{A}$. For buckling $\Delta = 0.78\mathring{A}$, the bandstrucutre at Γ-point for the lowest lying conduction band was found to be crossing the Fermi level and attaining a negative energy. For this purpose, we have shifted the bandstrucutre towards Fermi level so as to record the Dirac point at zero of energy in order to be able to compare the two bucking configurations. There is a stark difference between the energies of lowest lying conduction band and highest lying valance band at the Γ-point. However, the choice of parameters suggests that despite having a stable buckling configuration, figure (3.7(a)) is not a correct description of the band energies for silicene[5]. Forced by the imperfect

[4]The band structure for $\Delta = 0.78\mathring{A}$ has been shifted towards the Fermi level in order to differentiate between the two.

[5]It could possibly be due to the consideration of 2NN in the calculation. Though, the band structure produced here exactly matches with the intial work of Reference [21]

Material	$H_{ss\sigma}$	$H_{sp\sigma}$	$H_{pp\sigma}$	$H_{pp\pi}$	$\epsilon_s - \epsilon_p$
Silicene	-1.93	2.54	4.47	-1.12	-7.03
Germanene	-1.79	2.36	4.15	-1.04	-8.02
Stanene	-2.6245	2.6504	1.4926	-0.7877	-6.2335

Table 3.4: On-site and hopping parameter values for analogues of graphene from group IV. Adapted from Ref. [39, 40]

selection of parameters, we moved on to another set of parameters(table 3.4) and followed the same reference for germanene and stanene as well.

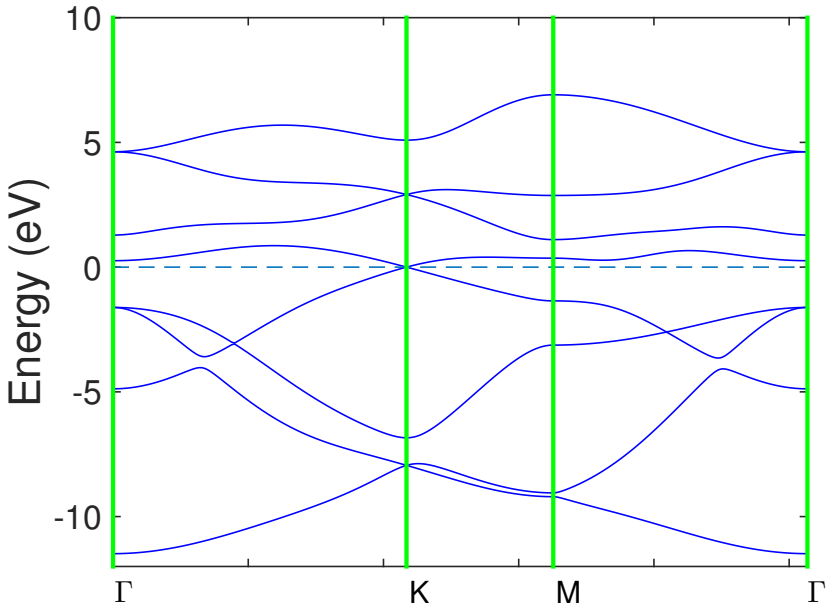

(a)

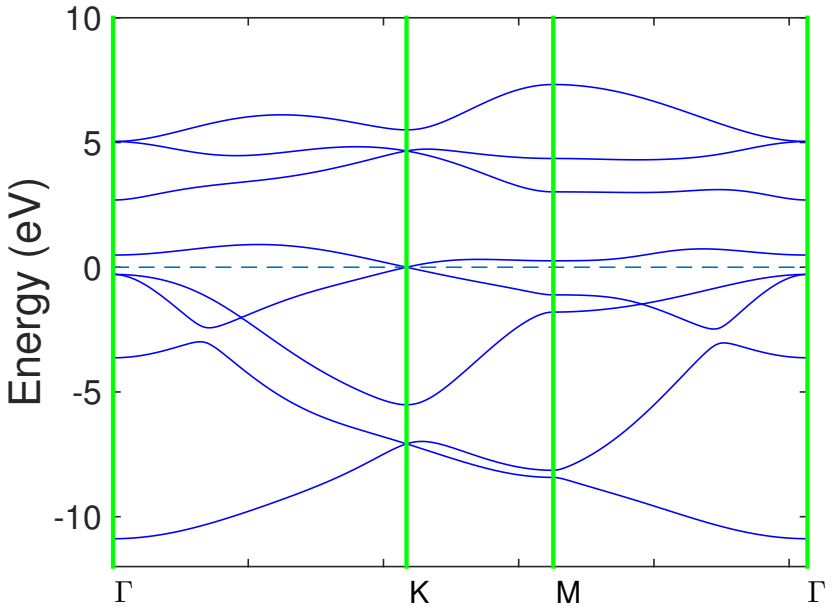

(b)

Figure 3.7: Electronic band structure of Silicene with buckling (a) 0.44$\mathring{A}$ and (b) 0.78$\mathring{A}$

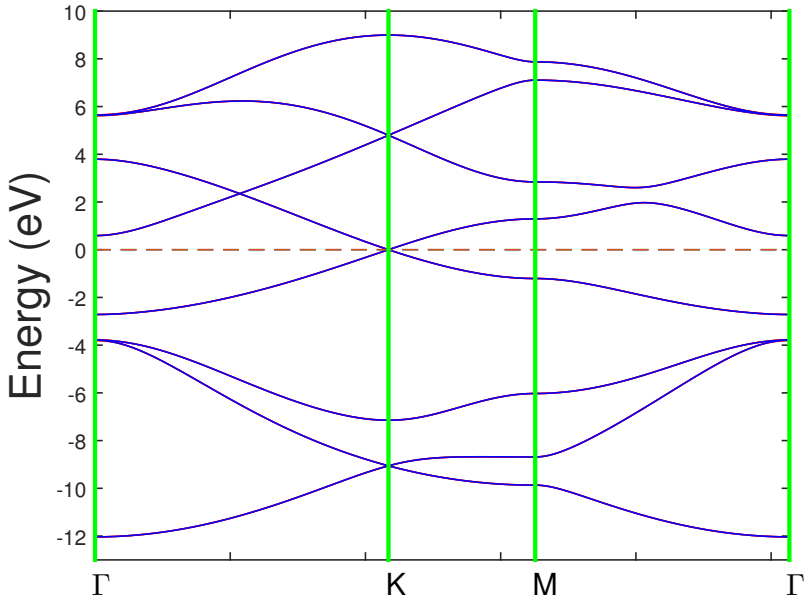

(a)

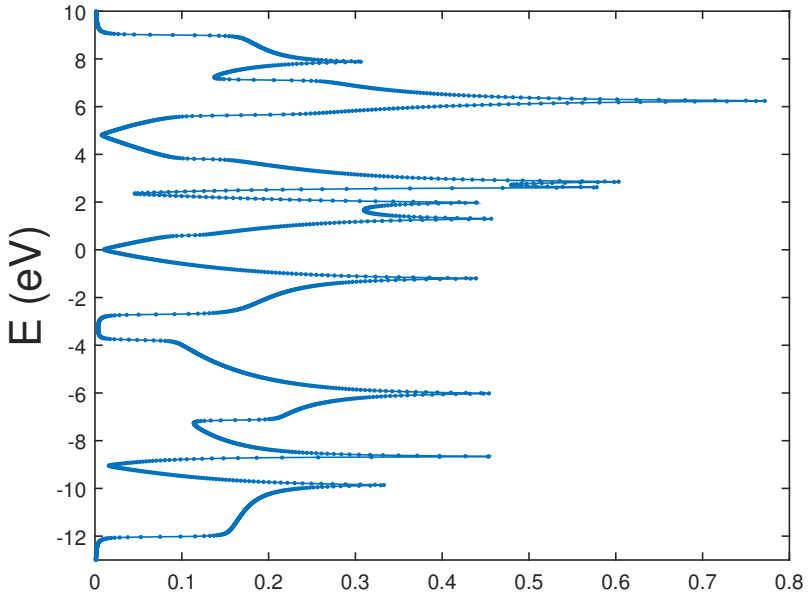

(b)

Figure 3.8: (a) Electronic band structure of Silicene with inclusion of spin-orbit coupling. The splitting of degenerate bands is not noticeable in the figure due to the smaller value of the strength of SOC. DOS in the energy range $(-13eV \leq E \leq 10eV)$. TB parameters used are as given in the table (3.4).

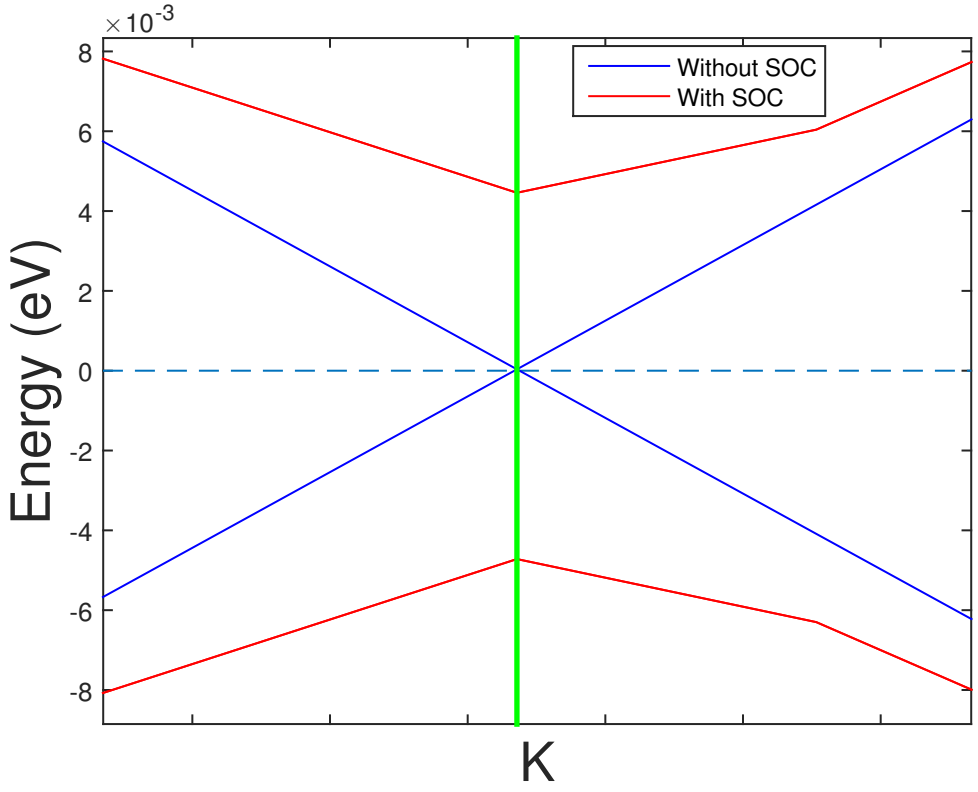

Figure 3.9: Electronic band structure of π bands in Silicene with inclusion of spin-orbit coupling

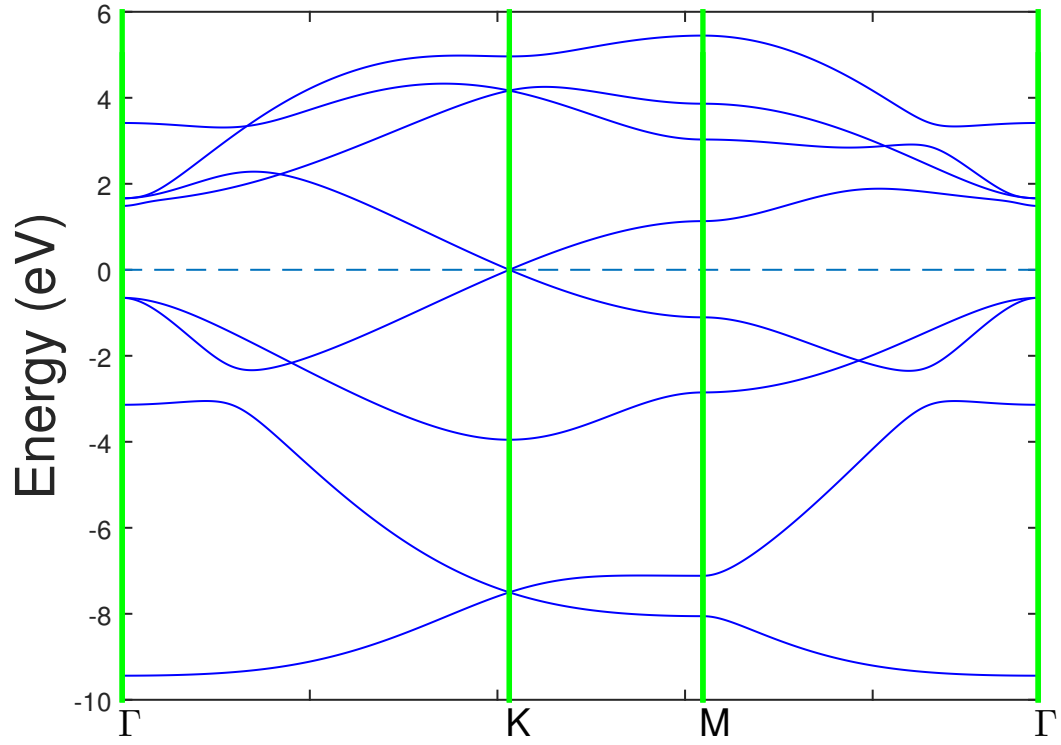

Figure 3.10: Electronic band structure of whole band Germanene without spin-orbit coupling

3.3 Electronic Properties of Germanene

Free standing germanene has a stable buckling in the z-direction within a range $0.64\mathring{A} \leq \Delta \leq 0.74\mathring{A}$ [41], depending on the approach. Buckling $\Delta = 0.64\mathring{A}$ plays an important role in deciding intrinsic electronic properties of germanene. In particular, the quasi-2D geometry supplemented by a strong SOC interaction paves way for a significant bandgap opening at the Dirac point. Figure (3.10) represents electronic band structure of germanene for 8 degenerate bands in a sp^3 hybridization scheme.

The tight binding model remains the same from equation (3.33) to equation (3.37) as for silicene, except for the parameters which are taken from table (3.4). It is interesting to note that highest occupied and lowest unoccupied bands are symmetric with respect to the Fermi level. Considering SOC splits up the bands and is presented in figure (3.11). A wide bandgap of 48 meV is observed at the Dirac point under the influence of spin-orbit interaction. At M point, the low lying bands exhibits a saddle-point with high electron densities.

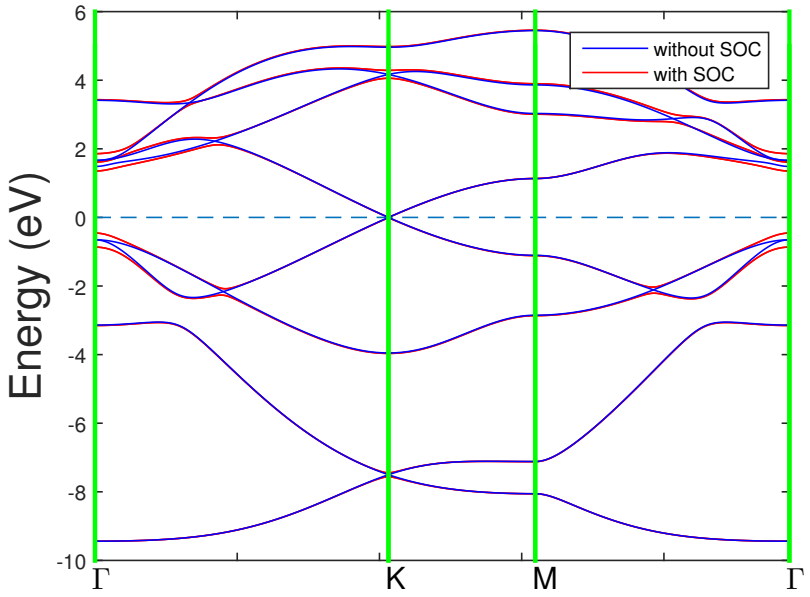

(a)

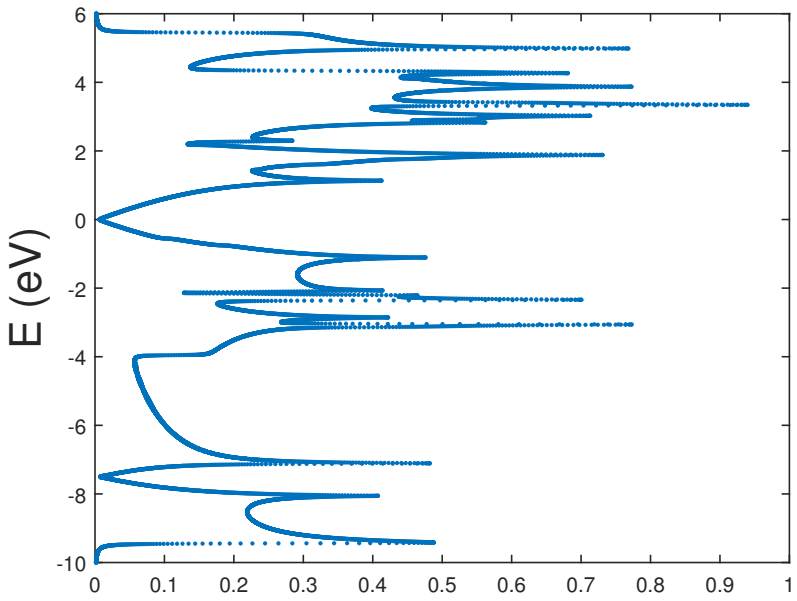

(b)

Figure 3.11: (a) Electronic band structure of whole band Germanene with inclusion of spin-orbit coupling and (b) DOS in the energy range ($-10eV \leq E \leq 6eV$).

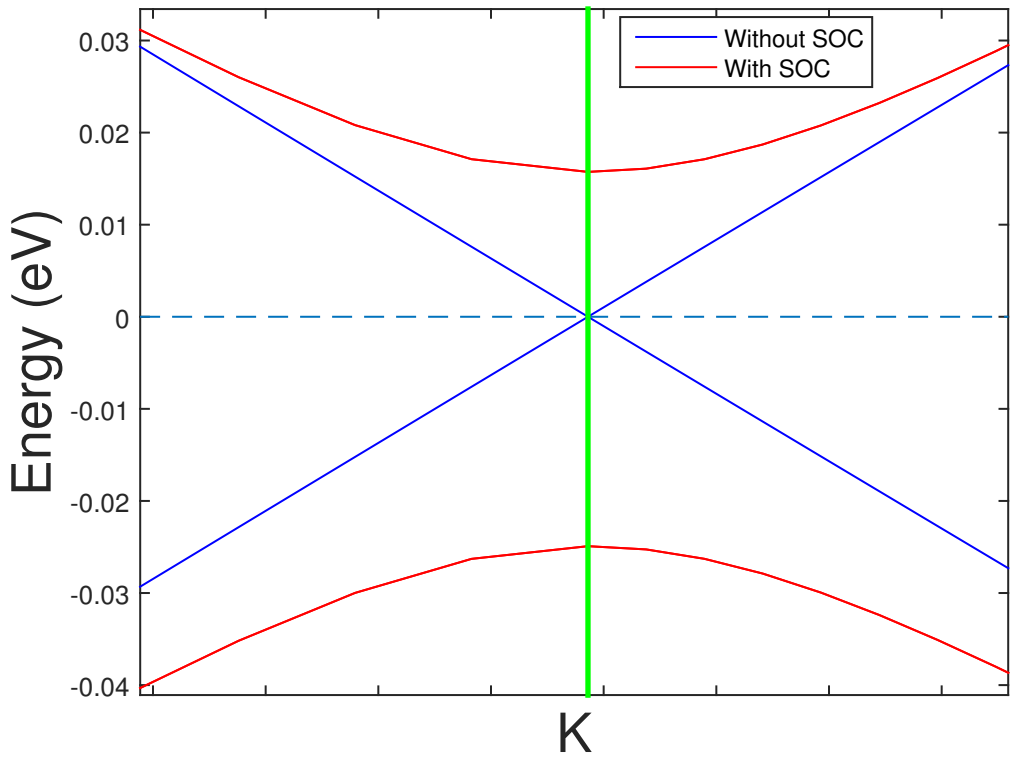

Figure 3.12: Electronic band structure of π bands in Germanene with inclusion of spin-orbit coupling

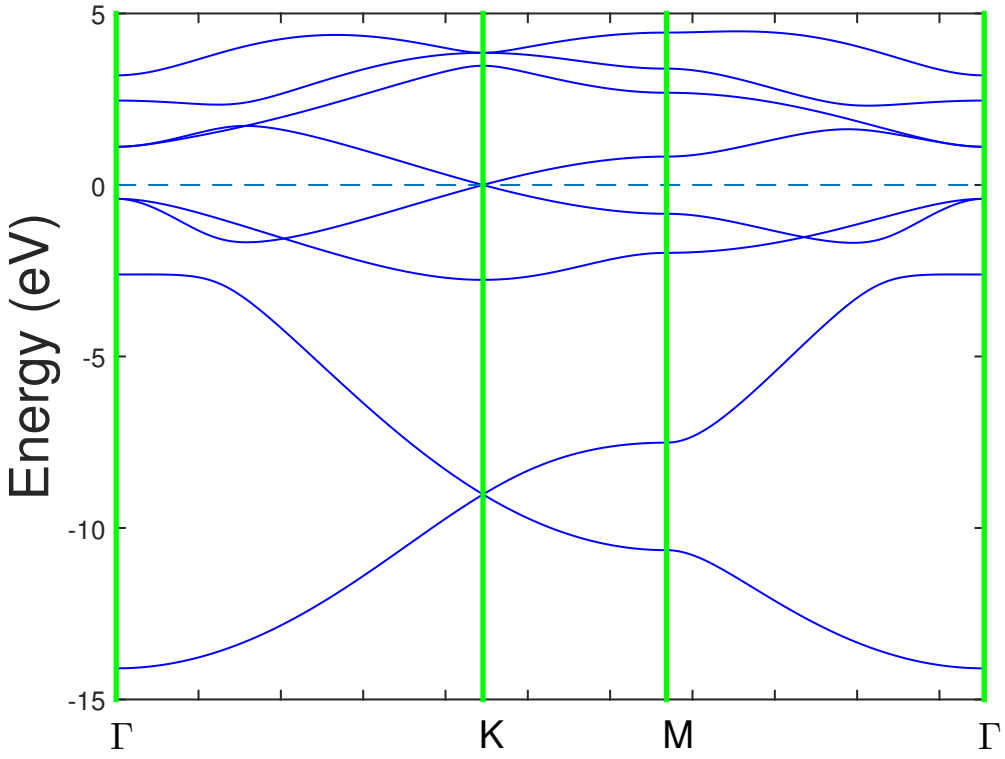

Figure 3.13: Electronic band structure of whole band Stanene without spin-orbit coupling

3.4 Electronic Properties of Stanene

Tin is heaviest among all structures studied in this thesis having an electronic configuration of $[Kr]\,4d^{10}5s^25p^2$. The hexagonal 2D honeycomb lattice structure of tin (stanene/tinene), similar to silicene and germanene, favors a sp^3 hybridized structure where all valance orbitals (namely $5s, 5p_x, 5p_y, 5p_z$) participate in the hybridization. Energy band structure of stanene is shown in figure (3.13) obtained from the tight binding model discussed in section (3.2). Introducing SOC into the model leads to significant splitting of bands as presented in figure (3.14.a). DOS is plotted in figure (3.14.b) in the energy range ($-3eV \leq E \leq 3eV$), where mainly $5p_x, 5p_y$ and $5p_z$ orbitals are responsible for hopping. Calculation of DOS

is done as

$$DOS\left(E\right)=\frac{1}{4\pi^{2}}\sum_{c,v}\iint_{1^{st}BZ}\frac{\gamma}{\pi}\frac{1}{\left(E-E_{c,v}\left(k_{x},k_{y}\right)\right)^{2}+\gamma^{2}}dk_{x}dk_{y} \tag{3.38}$$

where the energy dependent quantity in fraction in the integral is the definition of δ function.

In the absence of SOC, the Dirac cones at the vertices of first BZ remain gapless. The strength of SOC in stanene is 0.4 meV which in turn induces a significant gap of 0.13 eV at the K and $K^{'}$ points (figure(3.15)). The band structure maintains its behavior throughout except at Γ point, where a large splitting is observed to occur. The energy bands in stanene could further be classified as having three , namely linear at the K and $K^{'}$ points, parabolic around the band edge states and and partially flat regions around Γ point.

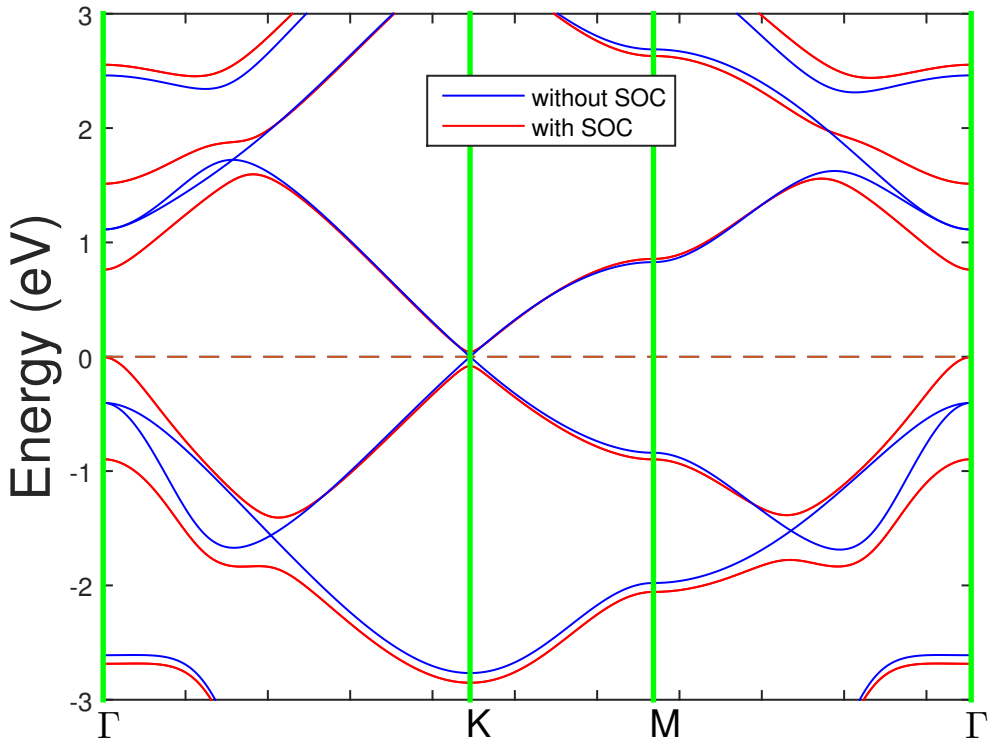

(a)

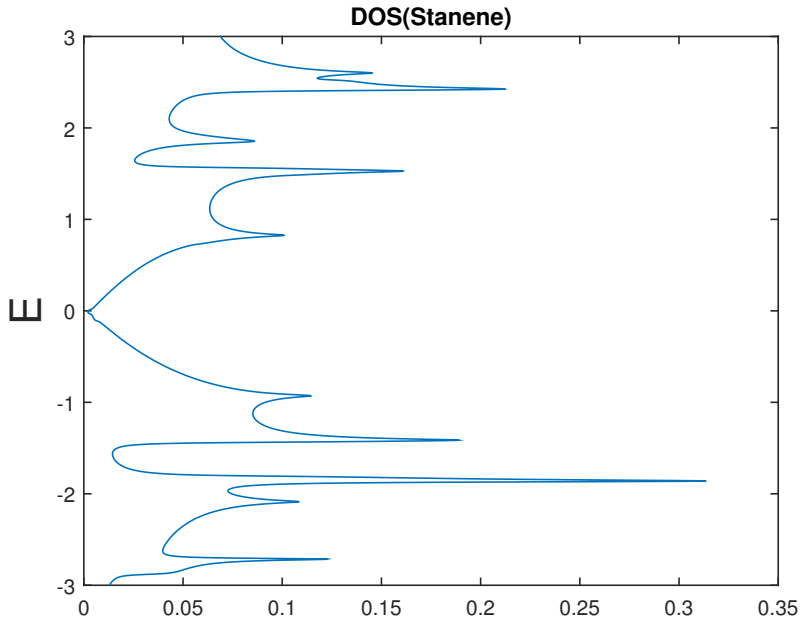

(b)

Figure 3.14: (a)Electronic band structure and of whole band Stanene with inclusion of spin-orbit coupling and(b) DOS in the energy range ($-3eV \leq E \leq 3eV$).

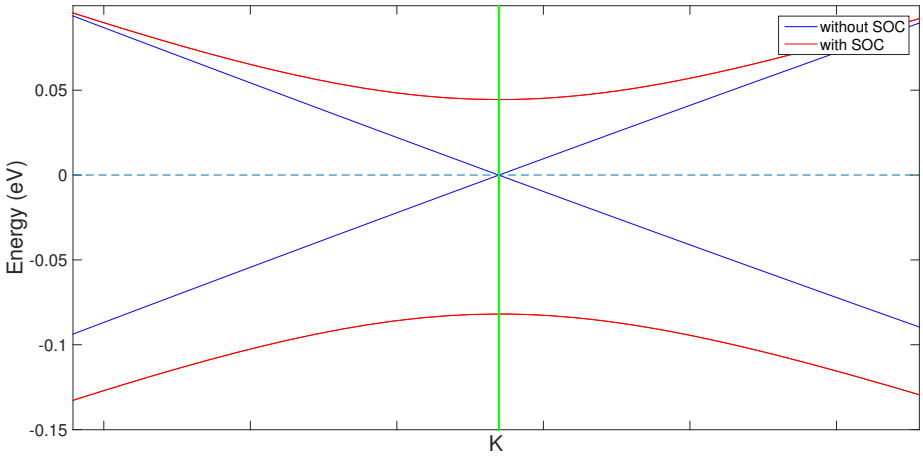

Figure 3.15: Electronic band structure of π bands in Stanene with inclusion of spin-orbit coupling

Chapter 4

Optical properties of 2D materials

Measuring optical absorption is probably one of the most simplest and direct approach to explore the band structure of a semiconductor or a metallic material. Computing and analyzing the electronic band structure data therefore plays a significant role in characterizing a material. Optical absorption is defined as a process in which an electron from the valance bands makes a transition to the conduction bands by virtue of absorbing a photon with sufficient energy. For transitions in which the valance band maxima and conduction band minima lie at the same k-point are symbolized as direct transitions and all other transitions fall in the category of indirect transitions.

In this chapter, we constrained ourselves to study direct transitions between the occupied valance and empty conduction bands for 2D class of materials discussed in the previous chapter. Calculation of optical properties is primarily dependent on the momentum matrix element (MME) as a signature of the optical transition. Within the sp^3 hybridization scheme, 8 degenerate energy bands are taken into account for calculating the values of MME.

4.1 Optical Absorption

Calculation of frequency (ω) dependent optical absorption is derived from Fermi's golden rule and is given as [24]

$$A(\omega) \propto \sum_{c,v,n,n'} \int\int_{1stBZ} \frac{dk_x dk_y}{(2\pi)^2} \left| \left\langle \Psi_{c,n'}(k_x,k_y) | \frac{\hat{E}.\mathbf{P}}{m_e} | \Psi_{v,n}(k_x,k_y) \right\rangle \right|^2 \times Im\left[\frac{f\left(E^c_{n'}(k_x,k_y)\right) - f\left(E^v_n(k_x,k_y)\right)}{E^c_{n'}(k_x,k_y) - E^v_n(k_x,k_y) - (\omega + i\gamma)} \right] \tag{4.1}$$

where the integration is carried throughout the first BZ spanned in two dimensions by k_x and k_y, c and v denotes the conduction and valance band respectively, n and n' symbolizes the nth band measured from the Fermi level towards the valance and conduction bands respectively. $f\left(E^{v,c}_{n,n'}(k_x,k_y)\right)$ is the Fermi-Dirac distribution function which assumes a value of either 0 or 1 at zero temperature. $E^{v,c}_{n,n'}(k_x,k_y)$ is the eigen energy and $\Psi_{v,c,n,n'}(k_x,k_y)$ is the wave function which are obtained by diagonalizing the TB Hamiltonian matrix. Within the momentum matrix element, $\hat{E}$ denotes the electric polarization vector with and $\mathbf{P}$ is momentum operator. The choice of broadening parameter γ is flexible and varies for material under consideration[1].

Calculation of MME (let's call it $\mathbf{P}_{vc}(k)$) in equation (4.1), depends on the direction of electric polarization vector $\hat{E}$. This alongside the dot product with momentum operator $\mathbf{P}$ defines two directions to investigate: (1) light field parallel to the plane ($\hat{E}$ lies in a plane spanned by k_x and k_y), (2) light field perpendicular to the plane (direction of $\hat{E}$ is parallel to k_z). In order to be able to calculate MME explicitly [25] for in-plane polarization, it can further be decomposed as

$$|P_{vc}(\mathbf{k})|^2 = \frac{1}{2}\left(|\langle c|P_x|v\rangle|^2 + |\langle c|P_y|v\rangle|^2 \right) \tag{4.2}$$

The n'th state could be written as

$$|n\rangle = \sum_{\alpha} c^n_\alpha |\alpha\rangle \tag{4.3}$$

[1]Generally, the value assigned to broadening parameter γ is very small (of the order of tens of meV)

where

$$\begin{aligned} |\alpha\rangle &= \frac{1}{\sqrt{N}} \sum_{N} e^{i\mathbf{k}.\mathbf{R}_i} \left|\pi^A_{\mathbf{R}_i}\right\rangle \\ |\beta\rangle &= \frac{1}{\sqrt{N}} \sum_{N} e^{i\mathbf{k}.\mathbf{R}_j} \left|\pi^B_{\mathbf{R}_j}\right\rangle \end{aligned} \tag{4.4}$$

Considering $\mathbf{P}_x$ to be momentum matrix in x-direction, with $\mathbf{c}$ and $\mathbf{v}$ being the conduction and valance state eigenvectors, MME's can be written as

$$\langle c|P_x|v\rangle = \sum_{\alpha,\beta} c^{c*}_{\alpha} c^{v}_{\beta} \langle\alpha|P_x|\beta\rangle = \mathbf{c}^{\dagger}\mathbf{P}_x\mathbf{v} \tag{4.5}$$

The commutation relation of Hamiltonian operator H and position operator $\mathbf{x}$ can be given as

$$[H, \mathbf{x}] = \frac{\hbar}{im}\mathbf{P}_x \tag{4.6}$$

therefore

$$\begin{aligned} \langle\alpha|\mathbf{P}_x|\beta\rangle &= \frac{im}{\hbar} \langle\alpha|[H, \mathbf{x}]|\beta\rangle \\ &= \frac{im}{\hbar} \left(\langle\alpha|H\mathbf{x}|\beta\rangle - \langle\alpha|\mathbf{x}H|\beta\rangle\right) \end{aligned} \tag{4.7}$$

The completeness of p_z states can be written as

$$\sum_i \left|\pi^A_{R_i}\right\rangle \left\langle\pi^A_{R_i}\right| + \sum_j \left|\pi^B_{R_j}\right\rangle \left\langle\pi^B_{R_j}\right| = 1 \tag{4.8}$$

Equation (4.6) then assumes the form

$$\begin{aligned} \langle\alpha|\mathbf{P}_x|\beta\rangle = \frac{im}{\hbar} \Bigg(&\sum_i \left(\left\langle\alpha|H|\pi^A_{R_i}\right\rangle \left\langle\pi^A_{R_i}|\mathbf{x}|\beta\right\rangle - \left\langle\alpha|\mathbf{x}|\pi^A_{R_i}\right\rangle \left\langle\pi^A_{R_i}|H|\beta\right\rangle\right) \\ &+ \sum_j \left(\left\langle\alpha|H|\pi^B_{R_j}\right\rangle \left\langle\pi^B_{R_j}|\mathbf{x}|\beta\right\rangle - \left\langle\alpha|\mathbf{x}|\pi^B_{R_j}\right\rangle \left\langle\pi^B_{R_j}|H|\beta\right\rangle\right) \end{aligned} \tag{4.9}$$

If only on-site terms were supposed to contribute, then $\left\langle\alpha|\mathbf{x}|\pi^B_{R_j}\right\rangle = \left\langle\pi^A_{R_i}|\mathbf{x}|\beta\right\rangle = 0$, $\left\langle\alpha|\mathbf{x}|\pi^A_{R_i}\right\rangle = \frac{1}{\sqrt{N}} R^A_i e^{-i\mathbf{k}.\mathbf{R}^A_i}$ and $\left\langle\pi^B_{R_j}|x|\beta\right\rangle = \frac{1}{\sqrt{N}} R^B_j e^{i\mathbf{k}.\mathbf{R}^B_j}$, where R^A_i and R^B_i are the x-coordinates of vectors $\mathbf{R}^A_i$ and $\mathbf{R}^B_i$. Using this, equation (4.8) then can be rewritten as

$$\begin{aligned} \langle\alpha|\mathbf{P}_x|\beta\rangle = &- \frac{im}{\hbar} \sum_i \left(\frac{1}{\sqrt{N}} R^A_i e^{-i\mathbf{k}.R^A_i} \left\langle\pi^A_{R_i}|H|\beta\right\rangle\right) \\ &+ \frac{im}{\hbar} \sum_j \left(\frac{1}{\sqrt{N}} R^B_j e^{i\mathbf{k}.R^B_j} \left\langle\alpha|H|\pi^B_{R_j}\right\rangle\right) \end{aligned} \tag{4.10}$$

It is straightforward then to write $R_i^A e^{-i\mathbf{k}.\mathbf{R}_i^A} = i\frac{\partial}{\partial k_x} e^{-i\mathbf{k}.\mathbf{R}_i^A}$ and $R_j^B e^{i\mathbf{k}.\mathbf{R}_j^B} = -i\frac{\partial}{\partial k_x} e^{-i\mathbf{k}.\mathbf{R}_j^B}$. Equation (4.9) then reduces to

$$\begin{aligned}\langle\alpha|\mathbf{P}_x|\beta\rangle = \frac{im}{\hbar\sqrt{N}} \Bigg(\sum_i \left(\frac{\partial}{\partial k_x} \left(e^{-i\mathbf{k}.\mathbf{R}_i^A} \right) \langle \pi_{R_i}^A | H | \beta \rangle \right) \\ + \sum_j \left(\left\langle \alpha | H | \pi_{R_j}^B \right\rangle \frac{\partial}{\partial k_x} \left(e^{i\mathbf{k}.\mathbf{R}_j^B} \right) \right) \Bigg)\end{aligned} \tag{4.11}$$

Taking the partial derivatives inside the expectation values and some simplification returns equation (4.10) in a form

$$\begin{aligned}\langle\alpha|\mathbf{P}_x|\beta\rangle &= \frac{im}{\hbar} \left(\left\langle \frac{\partial\alpha}{\partial k_x} | H | \beta \right\rangle + \left\langle \alpha | H | \frac{\partial\beta}{\partial k_x} \right\rangle \right) \\ &= \frac{m}{\hbar} \frac{\partial}{\partial k_x} \langle\alpha|H|\beta\rangle\end{aligned} \tag{4.12}$$

Therefore, one may write the x-component of MME as

$$\mathbf{P}_x = \frac{m}{\hbar} \frac{\partial \mathbf{H}}{\partial k_x} \tag{4.13}$$

Similarly the y-component may be written as

$$\mathbf{P}_y = \frac{m}{\hbar} \frac{\partial \mathbf{H}}{\partial k_y} \tag{4.14}$$

Knowing the Hamiltonian matrix elements, it is easier to find its gradient with respect to k_x and k_y to calculate the values of MME. Figure (4.1) represents the interband optical absorption spectra of graphene within the graident approximation method. It is interesting to note that in the energy band structure of graphene, it does not have any low lying energy bands[2] near the Γ point. However at M point, an optical transition occurs from M_1 valance to M_1 conduction band having photon energy equal to nearly 6 eV[3]. In the limit when photon energy

[2]Low lying optical transitions are not observed in graphene (fig. 4.1) due to absence of such bands which could promote an electron from the valance band to the conduction band.

[3]High energy transitions do exist, but throughout this study we have limited our discussion to the low and mid-frequency spectra.

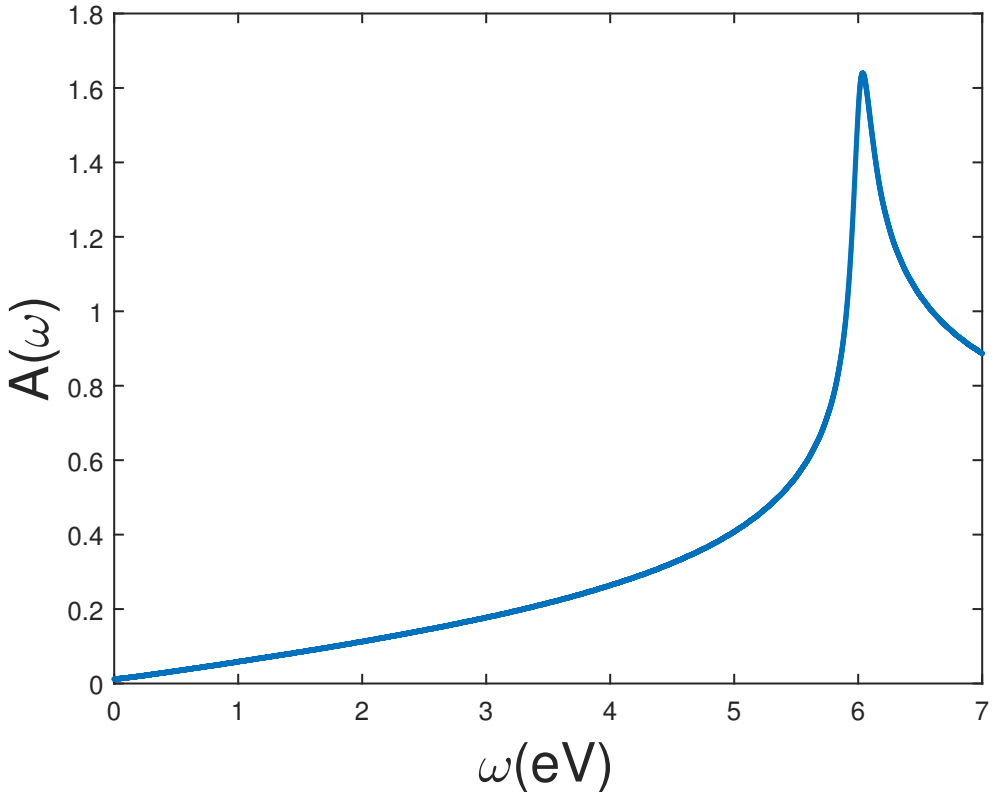

Figure 4.1: Optical absorption spectra (in arbitrary units) of graphene for light polarized parallel to the plane. An evident peak is observable at around 6 eV and is attributed to $M_{1\to1}$ transition.

is tending towards zero, theoretical calculation predicts [27] absorbance to be $A(0) = \pi\alpha = 0.0229136$, where $\alpha = \frac{e^2}{\hbar c}$ is the fine structure constant. Our result for graphene, $A(0) = 0.02290$ is in good agreement with experimental results [26] and theoretical prediction.

Optical absorption for silicene is shown in figure (4.2), where in the mid-frequency region three major peaks are observed. The first peak at 2.5 eV is due to a $M_{1\to1}$ transition in the energy band structure. An interesting feature of this peak is its symmetry on both sides, which is mainly due to the symmetric dispersion of $\pi\,(\pi^*)$ bonding (antibonding) bands below (above) the Fermi level. No other peak in the spectra is observed before this value (even after taking the SOC into account a 1.9 meV wide bandgap opens up at the Dirac point, which is not noticeable in the absorption spectra), however, the $M_{1\to1}$ transition could be shifted towards the zero of energy by the application of an external electric field [28]. In the absorption spectra, there are two other evident peaks at 4 eV and 4.5 eV corresponding to $M_{1\to2}$ and $\Gamma_{1\to1}$ transitions respectively. After the third peak at 4.5 eV, the spectrum attains a broader form due to an availability of wide bandwidth energy range in the σ and σ^* states. It is the difference of conduction and valance band energies at a given k-point $(E_c(k) - E_v(k))$, that dictates the interband transition. It is worth mentioning that, the peaks and shoulder structures in the absorption spectra $A(\omega)$ are related to the maxima, minima and saddle points (van Hove singularities) in the energy band structure of the material.

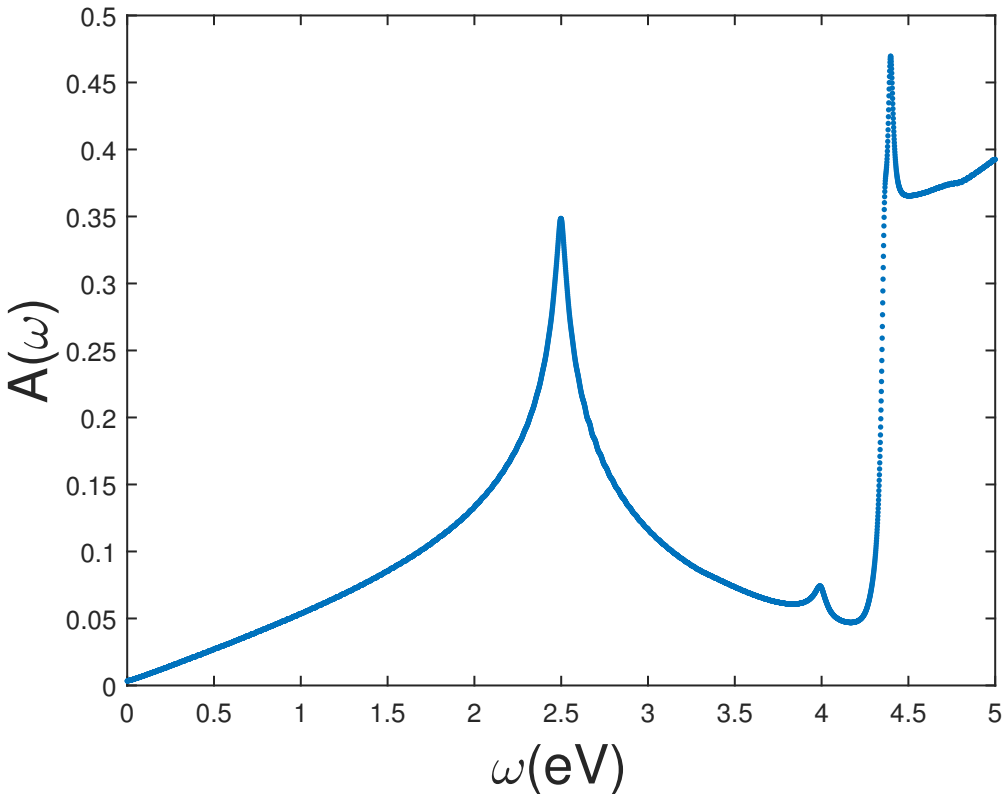

Figure 4.2: Optical absorption spectra (in arbitrary units) of silicene for light polarized parallel to the plane.

Figure (4.3) presents optical absorption spectra for germanene in the mid-frequency range for upto 5 eV of energy. Again, no low-energy peaks are observable suggesting the splitting around the Dirac point is very small[4]. However, a peak is observed at approximately 2.6 eV of photon energy which is due to a transition from M_1 valance band to the M_1 conduction band. Two consecutive peaks at 3.6 eV and 3.8 eV are observed next, which corresponds to a transition at the Γ point from $\Gamma_{1\to1}$ and $\Gamma_{1\to2}$ respectively. It is followed by a shoulder structure in the spectrum, which could be attributed to higher energy transitions taking place again at the Γ point but for transitions like $\Gamma_{2\to2}$ and so on.

[4]It does have a significant value, but in respect to high energy spectra they are negligible

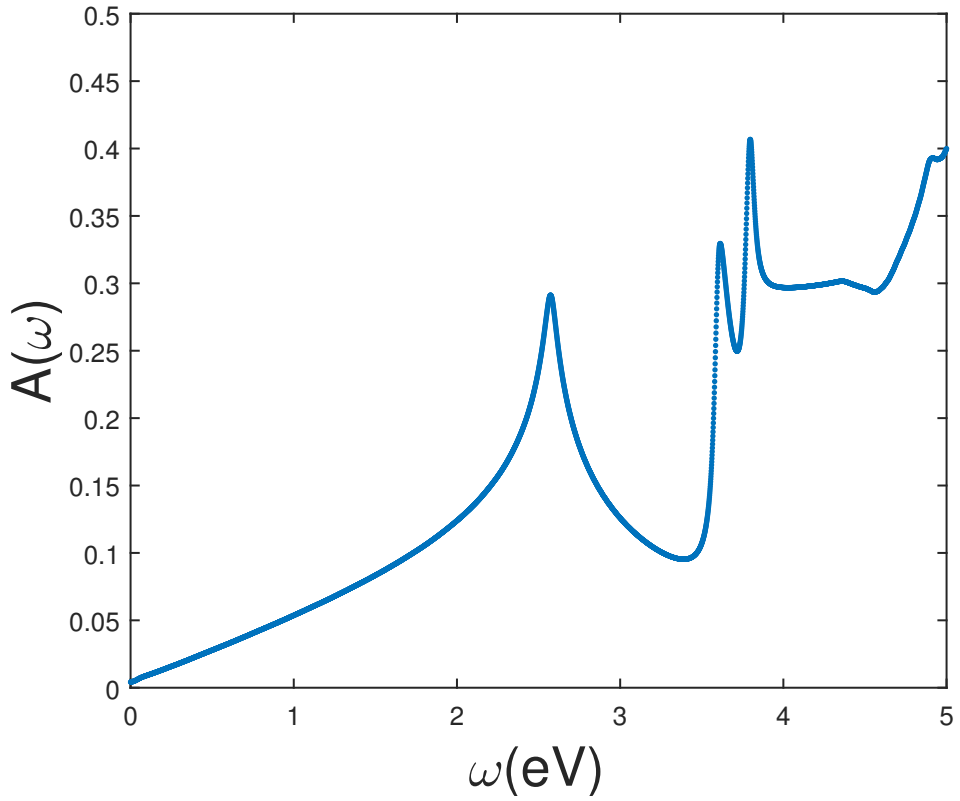

Figure 4.3: Optical absorption spectra (in arbitrary units) of germanene for in-plane polarization.

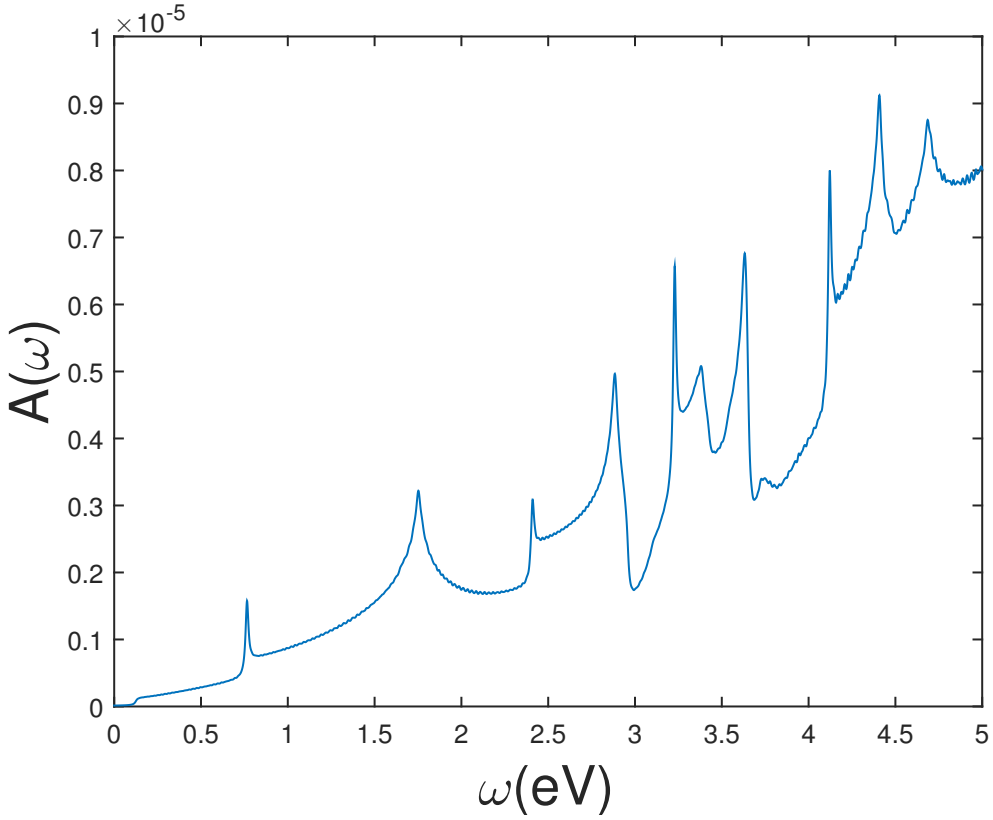

Figure 4.4: Optical absorption spectra (in arbitrary units) of stanene for in-plane polarization.

In figure (3.14), electronic band structure and density of states are plotted for stanene, where a significant wide bandgap of 0.13 eV value is opened up at the Dirac point. Broadening parameter γ takes a value of 10 meV for plotting the absorption spectra $A(\omega)$. The DOS plot clearly indicates 10 peaks featuring in the energy range of $-3eV \leq E \leq 3eV$. In the low energy region, due to SOC effect, a jump is visible at 0.13 eV in the absorption spectra $A(\omega)$ in figure (4.4). This jump resembles a transition from K_1 valance to the K_1 conduction band dominated by the $5p_z$ orbitals. An analysis of the band structure suggests, that the degeneracy at the Γ point is broken by the inclusion of SOC by a significant amount. Another peak in the low-energy region at 0.8 eV is due to $\Gamma_{1\to1}$ transition. A series of peaks are observed from 1.8 eV to 4.8 eV in the absorption spectra. These peaks are denominated as $M_{1\to1}$, $\Gamma_{2\to2}$, $C_{1\to1}$, $C_{1\to2}$, $C_{2\to1}$, $M_{1\to2}$, $C_{2\to2}$, $\Gamma_{3\to2}$, $C_{2\to3}$ and $M_{2\to2}$ respectively. Apart from high-symmetry points,

there are some saddle points (also called constant energy loops and are usually denoted as C transitions) and Van Hove singularities in the energy band structure of stanene (as can be seen in the form of peaks in the DOS).

Chapter 5

Conclusion

Tight binding model is an important tool for estimating the electronic band structure and properties of a material system. In this thesis, graphene and its 2D buckled analogues from group IV have been investigated. We have built up an analytical TB model which takes into account the buckling in the z-direction and have compared our results to the existing results. Different set of hopping and on-site parameters have been used for nearest and next-nearest neighbors to compare the accuracy of bandstrucutres. As a next step, this thesis includes spin-orbit coupling in such systems and a significant change in the bandstrucutre is seen to take place as we go down from $Graphene \rightarrow Silicene \rightarrow Germanene \rightarrow Stanene$. Opening of band gap at the Dirac point is reported which matches the existing values.

These feature rich 2D materials from the carbon family have been investigated for their optical properties. Together with gradient approximation method, we found excellent agreement of our results for the absorption spectra. Among all these materials, stanene has been found to have low lying energy bands in the energy band structure. It is the bulky size of Sn, that creates a better opportunity for an effective hopping between $5p_x$, $5p_y$ and $5p_z$ orbitals.

Considering the exotic properties exhibited by stanene, future work includes examining electronic and optical properties multilayer stanene and nanostructures made of stanene. Utilizing the model presented in this thesis, it is possible to extend it for such purposes. Another possible extension of this work is to investigate monolayer stanene on different substrates to explore its stability at room temperature. SOC effects could also be studied for measuring the competition between intrinsic and rashba SOC terms. Defects in the system could be introduced by means of Green's function, and its affect on the properties could be studied by moderately modifying the model.

Bibliography

[1] K. S. Novoselov, A. K. Geim, S. V. Morozov, D. Jiang, Y. Zhang, S. V. Dubonos, I. V. Grigorieva and A. A. Firsov, Electric field effect in atomically thin carbon films, Science, vol. 306, no. 5696, pp. 666-669, 2004.

[2] Philip Richard Wallace, The band theory of graphite, Physical Review, vol. 71, no. 9, pp. 622-634, 1947.

[3] JW McClure, Diamagnetism of graphite, Physical Review, vol. 104, no. 3, pp. 666-671, 1956.

[4] JC Slonczewski and PR Weiss, Band structure of graphite, Physical Review, vol. 109, no. 2, pp. 272-, 1958.

[5] K. S. Novoselov, D. Jiang, F. Schedin, T. J. Booth , V. V. Khotkevich, S. V. Morozov, and A. K. Geim, Two-dimensional atomic crystals, Proceedings of the National Academy of Sciences of the United States of America, vol. 102, no. 30, pp. 10451-10453, 2005.

[6] Andre K Geim and Konstantin S Novoselov, The rise of graphene, Nature materials, vol. 6, no. 3, pp. 183-191, 2007.

[7] Keun Soo Kim, Yue Zhao, Houk Jang, Sang Yoon Lee, Jong Min Kim, Kwang S. Kim, Jong-Hyun Ahn, Philip Kim, Jae-Young Choi and Byung Hee Hong, Large-scale pattern growth of graphene films for stretchable transparent electrodes, nature, vol. 457, no.7230, pp. 706, 2009.

[8] Novoselov K.S., Geim A.K., Morozov S.V., Jiang D., Katsnelson M.I., Grigorieva I.V., Dubonos S.V., Firsov A.A., Two-dimensional gas of massless Dirac fermions in graphene, nature, vol. 438, no.7065, pp. 197-200, 2005.

[9] Yenny Hernandez1, Valeria Nicolosi1, Mustafa Lotya1, Fiona M. Blighe1, Zhenyu Sun1, Sukanta De1, I. T. McGovern1, Brendan Holland1, Michele Byrne, Yurii K. Gun'Ko, John J. Boland, Peter Niraj, Georg Duesberg, Satheesh Krishnamurthy, Robbie Goodhue, John Hutchison, Vittorio Scardaci, Andrea C. Ferrari and Jonathan N. Coleman, High-yield production of graphene by liquid-phase exfoliation of graphite, Nature nanotechnology, vol. 3, no. 9, pp. 563-568, 2008.

[10] Nina I. Kovtyukhova, Yuanxi Wang, Ayse Berkdemir, Rodolfo Cruz-Silva, Mauricio Terrones, Vincent H. Crespi and Thomas E. Mallouk, Non-oxidative intercalation and exfoliation of graphite by Brønsted acids, Nature chemistry, vol. 6, no. 11, pp. 957-963, 2014.

[11] Pui Lam Chiu, Daniel D. T. Mastrogiovanni, Dongguang Wei, Cassandre Louis, Min Jeong, Guo Yu, Peter Saad, Carol R. Flach, Richard Mendelsohn, Eric Garfunkel, and Huixin He, Microwave-and nitronium ion-enabled rapid and direct production of highly conductive low-oxygen graphene, Journal of the American Chemical Society, vol. 134, no. 13, pp. 5850-5856, 2012.

[12] Mehulkumar Patel, Wenchun Feng, Keerthi Savaram, M. Reza Khoshi, Ruiming Huang, Jing Sun, Emann Rabie, Carol Flach, Richard Mendelsohn, Eric Garfunkel and Huixin He, Microwave Enabled One-Pot, One-Step Fabrication and Nitrogen Doping of Holey Graphene Oxide for Catalytic Applications, Small, vol. 11, no. 27, pp. 3358-3368, 2015.

[13] Mario Hofmann, Wan-Yu Chiang, Tuân D Nguyen and Ya-Ping Hsieh, Controlling the properties of graphene produced by electrochemical exfoliation, Nanotechnology, vol. 26, no. 33, pp. 335607, 2015.

[14] Yufei Mo, Yunfang Wan, Alicia Chau and Fuchuan Huang, Graphene/ionic liquid composite films and ion exchange, Scientific reports, vol. 4, 2014.

[15] Lars Matthes, Olivia Pulci and Friedhelm Bechstedt, Massive Dirac quasiparticles in the optical absorbance of graphene, silicene, germanene, and tinene, Journal of Physics: Condensed Matter, vol. 25, no. 39, pp. 395305, 2013.

[16] Gordon W Semenoff, Condensed-matter simulation of a three-dimensional anomaly, Physical Review Letters, vol. 53, no. 26, pp. 2449, 1984.

[17] F Duncan M Haldane, Model for a quantum Hall effect without Landau levels: Condensed-matter realization of the parity anomaly, Physical Review Letters, vol. 61, no. 18, pp. 2015, 1988.

[18] Rupali Kundu, Tight-binding parameters for graphene, Modern Physics Letters B, vol. 25, no. 03, pp. 163-173, 2011.

[19] Nathanael J. Roome, and J. David Carey, Beyond graphene: stable elemental monolayers of silicene and germanene, ACS applied materials & interfaces, vol. 6, no. 10, pp. 7743-7750, 2014.

[20] Seymur Cahangirov, Mehmet Topsakal, Ethem Aktürk, , H Şahin and Salim Ciraci, Two-and one-dimensional honeycomb structures of silicon and germanium, Physical Review Letters, vol. 102, no. 23, pp. 236804, 2009.

[21] Gian G Guzmán-Verri and LC Lew Yan Voon, Electronic structure of silicon-based nanostructures, Physical Review B, vol. 76, no. 7, pp. 075131, 2007.

[22] G Grosso and C Piermarocchi, Tight-binding model and interactions scaling laws for silicon and germanium, Physical Review B, vol. 51, no. 23, pp. 16772, 1995.

[23] AH Castro Neto, F Guinea, Nuno MR Peres, Kostya S Novoselov and Andre K Geim, The electronic properties of graphene, Reviews of modern physics, vol. 81, no. 1, pp. 109, 2009.

[24] Rong-Bin Chen, Szu-Chao Chen, Chih-Wei Chiu and Ming-Fa Lin, Optical properties of monolayer tinene in electric fields, Scientific Reports, vol. 7, 2009.

[25] Thomas Garm Pedersen, Kjeld Pedersen and Thomas Brun Kriestensen, Optical matrix elements in tight-binding calculations, Physical Review B, vol. 63, no. 20, pp. 201101, 2001.

[26] Kin Fai Mak, Matthew Y Sfeir, Yang Wu, Chun Hung Lui, James A Misewich and Tony F Heinz, Measurement of the optical conductivity of graphene, Physical Review Letters, vol. 101, no. 19, pp. 196405, 2008.

[27] Peter Y Yu and Manuel Cardona, Fundamentals of semiconductors: physics and materials properties, Springer, 2010.

[28] Suman Chowdhury and Debnarayan Jana, A theoretical review on electronic, magnetic and optical properties of silicene, Reports on Progress in Physics, vol. 79, no. 12, pp. 126501, 2016.

[29] Neil W Ashcroft and N David Mermin, Solid State Physics, Holt, Rinehart and Winston, New York, 1976.

[30] Adrian P Sutton, Electronic structure of materials, Clarendon Press, 1993.

[31] Walter A Harrison, Electronic structure and the properties of solids: the physics of the chemical bond, Courier Corporation, 2012.

[32] Riichiro Saito, Gene Dresselhaus and Mildred S Dresselhaus, Physical properties of carbon nanotubes, World scientific, 1998.

[33] Felix Bloch, Über die quantenmechanik der elektronen in kristallgittern, Zeitschrift für Physik A Hadrons and Nuclei, vol. 52, no. 7, pp. 555-600, 1929.

[34] John C Slater and George F Koster, Simplified LCAO method for the periodic potential problem, Physical Review, vol. 94, no. 6, pp. 1498, 1954.

[35] Behnaz Gharekhanlou and Sina Khorasani, An overview of tight-binding method for two-dimensional carbon structures, Graphene: Properties, Synthesis and Application, pp. 1-37, 2011.

[36] Efthimios Kaxiras, Atomic and electronic structure of solids, Cambridge University Press, 2003.

[37] Roland Winkler, Origin of Spin–Orbit Coupling Effects, Spin-Orbit Coupling Effects in Two-Dimensional Electron and Hole Systems, pp. 61-68, Springer, 2003.

[38] Lars Petersen and Per Hedegård, A simple tight-binding model of spin–orbit splitting of sp-derived surface states, Surface science, vol. 459, no. 1, pp. 49-56, 2000.

[39] Cheng-Cheng Liu, Hua Jiang and Yugui Yao, Low-energy effective Hamiltonian involving spin-orbit coupling in silicene and two-dimensional germanium and tin, Physical Review B, vol. 84, no. 19, pp. 195430, 2011.

[40] Yugui Yao, Fei Ye, Xiao-Liang Qi, Shou-Cheng Zhang and Zhong Fang, Spin-orbit gap of graphene: First-principles calculations, Physical Review B, vol. 75, no. 4, pp. 041401, 2007.

[41] Meng Ye, Ruge Quhe, Jiaxin Zheng, Zeyuan Ni, Yangyang Wang, Yakun Yuan, Geoffrey Tse, Junjie Shi, Zhengxiang Gao and Jing Lu, Tunable band gap in germanene by surface adsorption, Physica E: Low-dimensional Systems and Nanostructures, vol. 59, pp. 60-65, 2014.

Chapter 6

Appendix A

6.1 Dispersion Functions

$$\begin{aligned} g_0(\mathbf{k}) &= \sum_{j=1}^{3} e^{i\mathbf{k}.\delta_j^{(1)}} \\ &= e^{i\mathbf{k}.\delta_1^{(1)}} + e^{i\mathbf{k}.\delta_2^{(1)}} + e^{i\mathbf{k}.\delta_3^{(1)}} \end{aligned} \tag{6.1}$$

$$\begin{aligned} g_1(\mathbf{k}) &= \sum_{j=1}^{3} l_j^{(1)} e^{i\mathbf{k}.\delta_j^{(1)}} \\ &= l_1^{(1)} e^{i\mathbf{k}.\delta_1^{(1)}} + l_2^{(1)} e^{i\mathbf{k}.\delta_2^{(1)}} + l_3^{(1)} e^{i\mathbf{k}.\delta_3^{(1)}} \end{aligned} \tag{6.2}$$

$$\begin{aligned} g_2(\mathbf{k}) &= \sum_{j=1}^{3} m_j^{(1)} e^{i\mathbf{k}.\delta_j^{(1)}} \\ &= m_1^{(1)} e^{i\mathbf{k}.\delta_1^{(1)}} + m_2^{(1)} e^{i\mathbf{k}.\delta_2^{(1)}} + m_3^{(1)} e^{i\mathbf{k}.\delta_3^{(1)}} \end{aligned} \tag{6.3}$$

$$\begin{aligned} g_3(\mathbf{k}) &= \sum_{j=1}^{3} \left(l_j^{(1)}\right)^2 e^{i\mathbf{k}.\delta_j^{(1)}} \\ &= \left(l_1^{(1)}\right)^2 e^{i\mathbf{k}.\delta_1^{(1)}} + \left(l_2^{(1)}\right)^2 e^{i\mathbf{k}.\delta_2^{(1)}} + \left(l_3^{(1)}\right)^2 e^{i\mathbf{k}.\delta_3^{(1)}} \end{aligned} \tag{6.4}$$

$$\begin{aligned} g_4(\mathbf{k}) &= \sum_{j=1}^{3} [1 - \left(l_j^{(1)}\right)^2] e^{i\mathbf{k}.\delta_j^{(1)}} \\ &= [1 - \left(l_1^{(1)}\right)^2] e^{i\mathbf{k}.\delta_1^{(1)}} + [1 - \left(l_2^{(1)}\right)^2] e^{i\mathbf{k}.\delta_2^{(1)}} + [1 - \left(l_3^{(1)}\right)^2] e^{i\mathbf{k}.\delta_3^{(1)}} \end{aligned} \tag{6.5}$$

$$\begin{aligned} g_5(\mathbf{k}) &= \sum_{j=1}^{3} l_j^{(1)} m_j^{(1)} e^{i\mathbf{k}.\delta_j^{(1)}} \\ &= l_1^{(1)} m_1^{(1)} e^{i\mathbf{k}.\delta_1^{(1)}} + l_2^{(1)} m_2^{(1)} e^{i\mathbf{k}.\delta_2^{(1)}} + l_3^{(1)} m_3^{(1)} e^{i\mathbf{k}.\delta_3^{(1)}} \end{aligned} \tag{6.6}$$

$$\begin{aligned} g_6(\mathbf{k}) &= \sum_{j=1}^{3} \left(m_j^{(1)}\right)^2 e^{i\mathbf{k}.\delta_j^{(1)}} \\ &= \left(m_1^{(1)}\right)^2 e^{i\mathbf{k}.\delta_1^{(1)}} + \left(m_2^{(1)}\right)^2 e^{i\mathbf{k}.\delta_2^{(1)}} + \left(m_3^{(1)}\right)^2 e^{i\mathbf{k}.\delta_3^{(1)}} \end{aligned} \tag{6.7}$$

$$\begin{aligned} g_7(\mathbf{k}) &= \sum_{j=1}^{3} [1 - \left(m_j^{(1)}\right)^2] e^{i\mathbf{k}.\delta_j^{(1)}} \\ &= [1 - \left(m_1^{(1)}\right)^2] e^{i\mathbf{k}.\delta_1^{(1)}} + [1 - \left(m_2^{(1)}\right)^2] e^{i\mathbf{k}.\delta_2^{(1)}} + [1 - \left(m_3^{(1)}\right)^2] e^{i\mathbf{k}.\delta_3^{(1)}} \end{aligned} \tag{6.8}$$

$$\begin{aligned} g_8(\mathbf{k}) &= \sum_{j=1}^{3} n_j^{(1)} e^{i\mathbf{k}.\delta_j^{(1)}} \\ &= n_1^{(1)} e^{i\mathbf{k}.\delta_1^{(1)}} + n_2^{(1)} e^{i\mathbf{k}.\delta_2^{(1)}} + n_3^{(1)} e^{i\mathbf{k}.\delta_3^{(1)}} \end{aligned} \tag{6.9}$$

$$\begin{aligned} g_9(\mathbf{k}) &= \sum_{j=1}^{3} l_j^{(1)} n_j^{(1)} e^{i\mathbf{k}.\delta_j^{(1)}} \\ &= l_1^{(1)} n_1^{(1)} e^{i\mathbf{k}.\delta_1^{(1)}} + l_2^{(1)} n_2^{(1)} e^{i\mathbf{k}.\delta_2^{(1)}} + l_3^{(1)} n_3^{(1)} e^{i\mathbf{k}.\delta_3^{(1)}} \end{aligned} \tag{6.10}$$

$$\begin{aligned} g_{10}(\mathbf{k}) &= \sum_{j=1}^{3} m_j^{(1)} n_j^{(1)} e^{i\mathbf{k}.\delta_j^{(1)}} \\ &= m_1^{(1)} n_1^{(1)} e^{i\mathbf{k}.\delta_1^{(1)}} + m_2^{(1)} n_2^{(1)} e^{i\mathbf{k}.\delta_2^{(1)}} + m_3^{(1)} n_3^{(1)} e^{i\mathbf{k}.\delta_3^{(1)}} \end{aligned} \tag{6.11}$$

$$\begin{aligned} g_{11}(\mathbf{k}) &= \sum_{j=1}^{3} \left(n_j^{(1)}\right)^2 e^{i\mathbf{k}.\delta_j^{(1)}} \\ &= \left(n_1^{(1)}\right)^2 e^{i\mathbf{k}.\delta_1^{(1)}} + \left(n_2^{(1)}\right)^2 e^{i\mathbf{k}.\delta_2^{(1)}} + \left(n_3^{(1)}\right)^2 e^{i\mathbf{k}.\delta_3^{(1)}} \end{aligned} \tag{6.12}$$

$$\begin{aligned} g_{12}(\mathbf{k}) &= \sum_{j=1}^{3} [1 - \left(n_j^{(1)}\right)^2] e^{i\mathbf{k}.\delta_j^{(1)}} \\ &= [1 - \left(n_1^{(1)}\right)^2] e^{i\mathbf{k}.\delta_1^{(1)}} + [1 - \left(n_2^{(1)}\right)^2] e^{i\mathbf{k}.\delta_2^{(1)}} + [1 - \left(n_3^{(1)}\right)^2] e^{i\mathbf{k}.\delta_3^{(1)}} \end{aligned} \tag{6.13}$$

$$\begin{aligned} g_{13}(\mathbf{k}) &= \sum_{j=1}^{6} e^{i\mathbf{k}.\delta_j^{(2)}} \\ &= e^{i\mathbf{k}.\delta_1^{(2)}} + e^{i\mathbf{k}.\delta_2^{(2)}} + e^{i\mathbf{k}.\delta_3^{(2)}} + e^{i\mathbf{k}.\delta_4^{(2)}} + e^{i\mathbf{k}.\delta_5^{(2)}} + e^{i\mathbf{k}.\delta_6^{(2)}} \end{aligned} \tag{6.14}$$

$$\begin{aligned} g_{14}(\mathbf{k}) &= \sum_{j=1}^{6} l_j^{(2)} e^{i\mathbf{k}.\delta_j^{(2)}} \\ &= l_1^{(2)} e^{i\mathbf{k}.\delta_1^{(2)}} + l_2^{(2)} e^{i\mathbf{k}.\delta_2^{(2)}} + l_3^{(2)} e^{i\mathbf{k}.\delta_3^{(2)}} + l_4^{(2)} e^{i\mathbf{k}.\delta_4^{(2)}} + l_5^{(2)} e^{i\mathbf{k}.\delta_5^{(2)}} + l_6^{(2)} e^{i\mathbf{k}.\delta_6^{(2)}} \end{aligned} \tag{6.15}$$

$$g_{15}(\mathbf{k}) = \sum_{j=1}^{6} m_j^{(2)} e^{i\mathbf{k}.\delta_j^{(2)}}$$
$$= m_1^{(2)} e^{i\mathbf{k}.\delta_1^{(2)}} + m_2^{(2)} e^{i\mathbf{k}.\delta_2^{(2)}} + m_3^{(2)} e^{i\mathbf{k}.\delta_3^{(2)}} + m_4^{(2)} e^{i\mathbf{k}.\delta_4^{(2)}} + m_5^{(2)} e^{i\mathbf{k}.\delta_5^{(2)}} + m_6^{(2)} e^{i\mathbf{k}.\delta_6^{(2)}} \tag{6.16}$$

$$g_{16}(\mathbf{k}) = \sum_{j=1}^{6} \left(l_j^{(2)}\right)^2 e^{i\mathbf{k}.\delta_j^{(2)}}$$
$$= \left(l_1^{(2)}\right)^2 e^{i\mathbf{k}.\delta_1^{(2)}} + \left(l_2^{(2)}\right)^2 e^{i\mathbf{k}.\delta_2^{(2)}} + \left(l_3^{(2)}\right)^2 e^{i\mathbf{k}.\delta_3^{(2)}} \tag{6.17}$$
$$+ \left(l_4^{(2)}\right)^2 e^{i\mathbf{k}.\delta_4^{(2)}} + \left(l_5^{(2)}\right)^2 e^{i\mathbf{k}.\delta_5^{(2)}} + \left(l_6^{(2)}\right)^2 e^{i\mathbf{k}.\delta_6^{(2)}}$$

$$g_{17}(\mathbf{k}) = \sum_{j=1}^{6} [1 - \left(l_j^{(2)}\right)^2] e^{i\mathbf{k}.\delta_j^{(2)}}$$
$$= [1 - \left(l_1^{(2)}\right)^2] e^{i\mathbf{k}.\delta_1^{(2)}} + [1 - \left(l_2^{(2)}\right)^2] e^{i\mathbf{k}.\delta_2^{(2)}} + [1 - \left(l_3^{(2)}\right)^2] e^{i\mathbf{k}.\delta_3^{(2)}} \tag{6.18}$$
$$+ [1 - \left(l_4^{(2)}\right)^2] e^{i\mathbf{k}.\delta_4^{(2)}} + [1 - \left(l_5^{(2)}\right)^2] e^{i\mathbf{k}.\delta_5^{(2)}} + [1 - \left(l_6^{(2)}\right)^2] e^{i\mathbf{k}.\delta_6^{(2)}}$$

$$g_{18}(\mathbf{k}) = \sum_{j=1}^{6} l_j^{(2)} m_j^{(2)} e^{i\mathbf{k}.\delta_j^{(2)}}$$
$$= l_1^{(2)} m_1^{(2)} e^{i\mathbf{k}.\delta_1^{(2)}} + l_2^{(2)} m_2^{(2)} e^{i\mathbf{k}.\delta_2^{(2)}} + l_3^{(2)} m_3^{(2)} e^{i\mathbf{k}.\delta_3^{(2)}} \tag{6.19}$$
$$+ l_4^{(2)} m_4^{(2)} e^{i\mathbf{k}.\delta_4^{(2)}} + l_5^{(2)} m_5^{(2)} e^{i\mathbf{k}.\delta_5^{(2)}} + l_6^{(2)} m_6^{(2)} e^{i\mathbf{k}.\delta_6^{(2)}}$$

$$g_{19}(\mathbf{k}) = \sum_{j=1}^{6} \left(m_j^{(2)}\right)^2 e^{i\mathbf{k}.\delta_j^{(2)}}$$
$$= \left(m_1^{(2)}\right)^2 e^{i\mathbf{k}.\delta_1^{(2)}} + \left(m_2^{(2)}\right)^2 e^{i\mathbf{k}.\delta_2^{(2)}} + \left(m_3^{(2)}\right)^2 e^{i\mathbf{k}.\delta_3^{(2)}} \tag{6.20}$$
$$+ \left(m_4^{(2)}\right)^2 e^{i\mathbf{k}.\delta_4^{(2)}} + \left(m_5^{(2)}\right)^2 e^{i\mathbf{k}.\delta_5^{(2)}} + \left(m_6^{(2)}\right)^2 e^{i\mathbf{k}.\delta_6^{(2)}}$$

$$
\begin{aligned}
g_{20}(\mathbf{k}) &= \sum_{j=1}^{6} [1-(m_j^{(2)})^2] e^{i\mathbf{k}.\delta_j^{(2)}} \\
&= [1-(m_1^{(2)})^2] e^{i\mathbf{k}.\delta_1^{(2)}} + [1-(m_2^{(2)})^2] e^{i\mathbf{k}.\delta_2^{(2)}} + [1-(m_3^{(2)})^2] e^{i\mathbf{k}.\delta_3^{(2)}} \\
&+ [1-(m_4^{(2)})^2] e^{i\mathbf{k}.\delta_4^{(2)}} + [1-(m_5^{(2)})^2] e^{i\mathbf{k}.\delta_5^{(2)}} + [1-(m_6^{(2)})^2] e^{i\mathbf{k}.\delta_6^{(2)}}
\end{aligned} \tag{6.21}
$$

$$
\begin{aligned}
g_{21}(\mathbf{k}) &= \sum_{j=1}^{6} n_j^{(2)} e^{i\mathbf{k}.\delta_j^{(2)}} \\
&= n_1^{(2)} e^{i\mathbf{k}.\delta_1^{(2)}} + n_2^{(2)} e^{i\mathbf{k}.\delta_2^{(2)}} + n_3^{(2)} e^{i\mathbf{k}.\delta_3^{(2)}} + n_4^{(2)} e^{i\mathbf{k}.\delta_4^{(2)}} + n_5^{(2)} e^{i\mathbf{k}.\delta_5^{(2)}} + n_6^{(2)} e^{i\mathbf{k}.\delta_6^{(2)}}
\end{aligned} \tag{6.22}
$$

$$
\begin{aligned}
g_{22}(\mathbf{k}) &= \sum_{j=1}^{6} l_j^{(2)} n_j^{(2)} e^{i\mathbf{k}.\delta_j^{(2)}} \\
&= l_1^{(2)} n_1^{(2)} e^{i\mathbf{k}.\delta_1^{(2)}} + l_2^{(2)} n_2^{(2)} e^{i\mathbf{k}.\delta_2^{(2)}} + l_3^{(2)} n_3^{(2)} e^{i\mathbf{k}.\delta_3^{(2)}} \\
&+ l_4^{(2)} n_4^{(2)} e^{i\mathbf{k}.\delta_4^{(2)}} + l_5^{(2)} n_5^{(2)} e^{i\mathbf{k}.\delta_5^{(2)}} + l_6^{(2)} n_6^{(2)} e^{i\mathbf{k}.\delta_6^{(2)}}
\end{aligned} \tag{6.23}
$$

$$
\begin{aligned}
g_{23}(\mathbf{k}) &= \sum_{j=1}^{6} m_j^{(2)} n_j^{(2)} e^{i\mathbf{k}.\delta_j^{(2)}} \\
&= m_1^{(2)} n_1^{(2)} e^{i\mathbf{k}.\delta_1^{(2)}} + m_2^{(2)} n_2^{(2)} e^{i\mathbf{k}.\delta_2^{(2)}} + m_3^{(2)} n_3^{(2)} e^{i\mathbf{k}.\delta_3^{(2)}} \\
&+ m_4^{(2)} n_4^{(2)} e^{i\mathbf{k}.\delta_4^{(2)}} + m_5^{(2)} n_5^{(2)} e^{i\mathbf{k}.\delta_5^{(2)}} + m_6^{(2)} n_6^{(2)} e^{i\mathbf{k}.\delta_6^{(2)}}
\end{aligned} \tag{6.24}
$$

$$
\begin{aligned}
g_{24}(\mathbf{k}) &= \sum_{j=1}^{6} (n_j^{(2)})^2 e^{i\mathbf{k}.\delta_j^{(2)}} \\
&= (n_1^{(2)})^2 e^{i\mathbf{k}.\delta_1^{(2)}} + (n_2^{(2)})^2 e^{i\mathbf{k}.\delta_2^{(2)}} + (n_3^{(2)})^2 e^{i\mathbf{k}.\delta_3^{(2)}} \\
&+ (n_4^{(2)})^2 e^{i\mathbf{k}.\delta_4^{(2)}} + (n_5^{(2)})^2 e^{i\mathbf{k}.\delta_5^{(2)}} + (n_6^{(2)})^2 e^{i\mathbf{k}.\delta_6^{(2)}}
\end{aligned} \tag{6.25}
$$

$$
\begin{aligned}
g_{25}(\mathbf{k}) &= \sum_{j=1}^{6} [1-(n_j^{(2)})^2] e^{i\mathbf{k}.\delta_j^{(2)}} \\
&= [1-(n_1^{(2)})^2] e^{i\mathbf{k}.\delta_1^{(2)}} + [1-(n_2^{(2)})^2] e^{i\mathbf{k}.\delta_2^{(2)}} + [1-(n_3^{(2)})^2] e^{i\mathbf{k}.\delta_3^{(2)}} \\
&+ [1-(n_4^{(2)})^2] e^{i\mathbf{k}.\delta_4^{(2)}} + [1-(n_5^{(2)})^2] e^{i\mathbf{k}.\delta_5^{(2)}} + [1-(n_6^{(2)})^2] e^{i\mathbf{k}.\delta_6^{(2)}}
\end{aligned} \tag{6.26}
$$

Direction cosines[1]

$$
l_j^{(n)} = \frac{\widehat{i}.\delta_j^{(n)}}{|\delta_j^{(n)}|}, \quad m_j^{(n)} = \frac{\widehat{j}.\delta_j^{(n)}}{|\delta_j^{(n)}|}, \quad n_j^{(n)} = \frac{\widehat{k}.\delta_j^{(n)}}{|\delta_j^{(n)}|} \tag{6.27}
$$

$$
\begin{aligned}
l_1^{(1)} &= \frac{a}{\sqrt{a^2+3\Delta^2}} \\
l_2^{(1)} &= -\frac{a}{2\sqrt{a^2+3\Delta^2}} \\
l_3^{(1)} &= -\frac{a}{2\sqrt{a^2+3\Delta^2}}
\end{aligned}
$$

$$
\begin{aligned}
m_1^{(1)} &= 0 \\
m_2^{(1)} &= \frac{\sqrt{3}a}{2\sqrt{a^2+3\Delta^2}} \\
m_3^{(1)} &= -\frac{\sqrt{3}a}{2\sqrt{a^2+3\Delta^2}}
\end{aligned} \tag{6.28}
$$

$$
\begin{aligned}
n_1^{(1)} &= -\frac{\sqrt{3}\Delta}{2\sqrt{a^2+3\Delta^2}} \\
n_2^{(1)} &= -\frac{\sqrt{3}\Delta}{2\sqrt{a^2+3\Delta^2}} \\
n_3^{(1)} &= -\frac{\sqrt{3}\Delta}{2\sqrt{a^2+3\Delta^2}}
\end{aligned}
$$

[1] a is the lattice constant and Δ is the amount of buckling in the z-direction

$$
\begin{aligned}
l_1^{(2)} &= 0 \\
l_2^{(2)} &= 0 \\
l_3^{(2)} &= \frac{\sqrt{3}}{2} \\
l_4^{(2)} &= -\frac{\sqrt{3}}{2} \\
l_5^{(2)} &= \frac{\sqrt{3}}{2} \\
l_6^{(2)} &= -\frac{\sqrt{3}}{2}
\end{aligned}
$$

$$
\begin{aligned}
m_1^{(2)} &= 1 \\
m_2^{(2)} &= -1 \\
m_3^{(2)} &= -\frac{1}{2} \\
m_4^{(2)} &= \frac{1}{2} \\
m_5^{(2)} &= \frac{1}{2} \\
m_6^{(2)} &= -\frac{1}{2}
\end{aligned}
\tag{6.29}
$$

$$
\begin{aligned}
n_1^{(2)} &= 0 \\
n_2^{(2)} &= 0 \\
n_3^{(2)} &= 0 \\
n_4^{(2)} &= 0 \\
n_5^{(2)} &= 0 \\
n_6^{(2)} &= 0
\end{aligned}
$$

6.2 Spin-Orbit coupling Hamiltonian

$$\langle p_x\uparrow|\mathbf{L}.\mathbf{S}|p_y\uparrow\rangle = \left\langle p_x\uparrow|\hat{L}_z|p_y\uparrow\right\rangle = \frac{1}{2i}(\langle 1| + \langle -1|)\,\hat{L}_z(|\,1\rangle - |\,-1\rangle) = -i\hbar \quad (6.30)$$

$$\langle p_y\uparrow|\mathbf{L}.\mathbf{S}|p_x\uparrow\rangle = \left\langle p_y\uparrow|\hat{L}_z|p_x\uparrow\right\rangle = -\frac{1}{2i}(\langle 1| - \langle -1|)\,\hat{L}_z(|\,1\rangle + |\,-1\rangle) = i\hbar \quad (6.31)$$

$$\langle p_x\uparrow|\mathbf{L}.\mathbf{S}|p_z\downarrow\rangle = \left\langle p_x\uparrow|\hat{L}_-|p_z\downarrow\right\rangle = \frac{1}{\sqrt{2}}(\langle 1| + \langle -1|)\,\hat{L}_-(|\,0\rangle) = \hbar \quad (6.32)$$

$$\langle p_z\uparrow|\mathbf{L}.\mathbf{S}|p_x\downarrow\rangle = \left\langle p_z\uparrow|\hat{L}_-|p_x\downarrow\right\rangle = \frac{1}{\sqrt{2}}(\langle 0|)\,\hat{L}_-(|\,1\rangle + |\,-1\rangle) = -\hbar \quad (6.33)$$

$$\langle p_y\uparrow|\mathbf{L}.\mathbf{S}|p_z\downarrow\rangle = \left\langle p_y\uparrow|\hat{L}_-|p_z\downarrow\right\rangle = -\frac{1}{\sqrt{2}i}(\langle 1| - \langle -1|)\,\hat{L}_-(|\,0\rangle) = -i\hbar \quad (6.34)$$

$$\langle p_z\uparrow|\mathbf{L}.\mathbf{S}|p_y\downarrow\rangle = \left\langle p_z\uparrow|\hat{L}_-|p_y\downarrow\right\rangle = \frac{1}{\sqrt{2}i}(\langle 0|)\,\hat{L}_-(|\,1\rangle - |\,-1\rangle) = i\hbar \quad (6.35)$$

$$\langle p_x\downarrow|\mathbf{L}.\mathbf{S}|p_y\downarrow\rangle = -\left\langle p_x\downarrow|\hat{L}_z|p_y\downarrow\right\rangle = -\frac{1}{2i}(\langle 1| + \langle -1|)\,\hat{L}_z(|\,1\rangle - |\,-1\rangle) = -i\hbar \quad (6.36)$$

$$\langle p_y\downarrow|\mathbf{L}.\mathbf{S}|p_x\downarrow\rangle = -\left\langle p_y\downarrow|\hat{L}_z|p_x\downarrow\right\rangle = \frac{1}{2i}(\langle 1| - \langle -1|)\,\hat{L}_z(|\,1\rangle + |\,-1\rangle) = -i\hbar \quad (6.37)$$

$$\langle p_x\downarrow|\mathbf{L}.\mathbf{S}|p_z\uparrow\rangle = \left\langle p_x\downarrow|\hat{L}_+|p_z\uparrow\right\rangle = \frac{1}{\sqrt{2}}(\langle 1| + \langle -1|)\,\hat{L}_+(|\,0\rangle) = -\hbar \quad (6.38)$$

$$\langle p_z\downarrow|\mathbf{L}.\mathbf{S}|p_x\uparrow\rangle = \left\langle p_z\downarrow|\hat{L}_+|p_x\uparrow\right\rangle = \frac{1}{\sqrt{2}}(\langle 0|)\,\hat{L}_+(|\,1\rangle + |\,-1\rangle) = \hbar \quad (6.39)$$

$$\langle p_y\downarrow|\mathbf{L}.\mathbf{S}|p_z\uparrow\rangle = \left\langle p_y\downarrow|\hat{L}_+|p_z\uparrow\right\rangle = -\frac{1}{\sqrt{2}i}(\langle 1| - \langle -1|)\,\hat{L}_+(|\,0\rangle) = -i\hbar \quad (6.40)$$

$$\langle p_z\downarrow|\mathbf{L}.\mathbf{S}|p_y\uparrow\rangle = \left\langle p_z\downarrow|\hat{L}_+|p_y\uparrow\right\rangle = \frac{1}{\sqrt{2}i}(\langle 0|)\,\hat{L}_+(|\,1\rangle - |\,-1\rangle) = i\hbar \quad (6.41)$$

Rest all elements in the spin-orbit coupling matrix are zero.